Cretaceous Research 148 (2023) 105555

Contents lists available at ScienceDirect

Cretaceous Research

journal homepage: www.elsevier.com/locate/CretRes

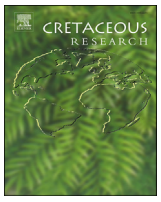

Cretaceous southern high latitude benthic foraminiferal assemblages during OAE 2 at IODP Site U1516, Mentelle Basin, Indian Ocean

E. Wolfgring [a, b, *], G. Amaglio [a], M.R. Petrizzo [a]

[a] Università Degli Studi di Milano, Department of Earth Sciences "A. Desio", Via Mangiagalli 34, 20133 Milano, Italy
[b] University of Vienna, Department of Palaeontology, Josef Holaubek Platz 2, 1090 Vienna, Austria

ARTICLE INFO

Article history:
Received 19 January 2023
Received in revised form
4 April 2023
Accepted in revised form 9 April 2023
Available online 11 April 2023

Keywords:
International Ocean Discovery Program
Benthic foraminifera
Cretaceous
Southern high latitudes
Oceanic Anoxic Event 2

ABSTRACT

At Site U1516 (Mentelle Basin, southeast Indian Ocean, offshore western Australia), the International Ocean Discovery Program (IODP) Expedition 369 recovered an almost complete pelagic record of the Upper Cretaceous, including the Oceanic Anoxic Event 2 (OAE 2). To better understand paleoenvironmental changes across OAE 2, 32 samples were analysed for benthic foraminiferal abundance data that represent one of the few benthic foraminiferal datasets spanning the OAE 2 in the southern high latitudes.

The OAE 2 interval at Site U1516 is characterized by an interval of low $CaCO_3$ content that contains a prominent positive Carbon Isotope Excursion (CIE). The record of the OAE 2 can be subdivided in pre OAE 2, pre max-CIE, low $CaCO_3$, and post low $CaCO_3$ intervals. Through the Cenomanian–Turonian boundary, we document an extreme decline in benthic foraminifera during OAE 2, that is followed by a profound repopulation event in the post low $CaCO_3$ interval.

Benthic foraminiferal assemblages indicate an outer neritic to upper bathyal depositional environment. During the pre OAE 2 and pre max-CIE intervals, calcareous deep-water gavelinellids, lingulogavelinellids and gyroidinids are dominant. In the low-carbonate interval, the microfossil record documents a substantial increase in radiolaria and foraminifera are almost absent as only three out of nine samples contain benthic foraminifera. Changes in benthic foraminiferal assemblage composition are documented in the initial low $CaCO_3$ interval, underlying the maximum CIE and associated interferences. Comparison of the pre- and post-CIE benthic foraminiferal assemblages highlights a distinct repopulation event during the post max- CIE interval mainly represented by the conspicuous increase in abundance of agglutinated taxa and *Conorboides*. Compared to other southern high latitude records, the dataset collected at Site U1516 represents one of the most complete benthic foraminiferal records across the OAE 2 that registers the Late Cretaceous environmental changes in the Southern Hemisphere.

1. Introduction

The Cenomanian–Turonian transition cannot be approached without discussing the perturbances in the ocean climate system recorded during the Oceanic Anoxic Event 2 (OAE 2) (e.g., Schlanger and Jenkyns, 1976; Scholle and Arthur, 1980; Schlanger et al., 1987). Elevated levels of CO_2 in the atmosphere resulted in ice-free poles and contributed to a weak meridional temperature gradient and an increasingly active hydrologic cycle (Poulsen et al., 1999; Forster et al., 2007; Sinninghe Damsté et al., 2010; Chen et al., 2022, 2023). The OAE 2 interval is characterized by a prominent positive Carbon Isotope Excursion (CIE) and often by an associated low carbonate interval documented in the sedimentary record, that was accompanied by an unprecedented rise in ocean temperatures (Scholle and Arthur, 1980; Tsikos et al., 2004; Voigt et al., 2006, 2008; Jenkyns, 2010; Friedrich et al., 2012; Jenkyns et al., 2017; Kuhnt et al., 2017). These events were probably triggered by massive CO_2 discharge that might be related to the emplacement of the High Arctic Large Igneous Province and/or Caribbean Large Igneous Province that emitted greenhouse gases, leading to the onset of the Cenomanian–Turonian Thermal Maximum. The enhancement of ocean fertility was accompanied by a rise in surface-ocean temperatures (to ~36 °C at high latitudes) and the

* Corresponding author.
E-mail addresses: erik.wolfgring@guest.unimi.it, erik.wolfgring@univie.ac.at (E. Wolfgring).

https://doi.org/10.1016/j.cretres.2023.105555

reduction of surface water latitudinal temperature gradients (Barclay et al., 2010; Du Vivier et al., 2014a; Erba, 2004; Jenkyns, 2003; Kuroda et al., 2007; Kuypers et al., 2002; Larson, 1991; Leckie et al., 2002; Pancost et al., 2004; Trabucho Alexandre et al., 2010; Turgeon and Creaser, 2008; Zheng et al., 2013). Regionally, the continuously increasing ocean temperatures during the OAE 2 interval are briefly interrupted by the Plenus Cold Event that has been attributed to a decrease in atmospheric pCO_2 forced by the widespread burial of organic carbon (Voigt et al., 2006; Barclay et al., 2010; Sinninghe Damsté et al., 2010; Jarvis et al., 2011; van Bentum et al., 2012; Gale et al., 2019; O'Connor et al., 2020).

During the extensive burial of organic matter and the global sea level highstand, and associated changes, benthic communities experienced severe restrictions (e.g.., Gertsch et al., 2010; Haq, 2014; Haq et al., 1987; Keller et al., 2021; Miller et al., 2005). Most records of carbon burial and environmental changes during OAE 2 have been obtained from sediments in the low latitudes of the Atlantic Ocean, the Tethyan region, and the Western Interior Seaway (e.g., Bomou et al., 2013; Bowman and Bralower, 2005; Caron et al., 2006; Desmares et al., 2016; Du Vivier et al., 2014; Elderbak and Leckie, 2016; Eldrett et al., 2014; Forster et al., 2008; Gale et al., 2019; Grosheny et al., 2017; Heimhofer et al., 2018; Jarvis et al., 2011; Kuhnt et al., 2017; Mort et al., 2007; Owens et al., 2013, 2013; Parente et al., 2008; Robinson et al., 2017; Sageman et al., 2006; Takashima et al., 2009; Tsikos et al., 2004; van Bentum et al., 2012; Voigt et al., 2008 among many others). To date, only few isolated records documenting the expression of OAE 2 from the Austral Realm and the southern high latitudes have been described as follows: Carnarvon basin (Haig et al., 2004), New Zealand (Hasegawa et al., 2013; Gangl et al., 2019), Kerguelen Plateau (Dickson et al., 2017), Exmouth Plateau (Rullkötter et al., 1992; Thurow et al., 2013), Cauvery Basin (Govindan and Ramesh 1995; Tewari et al., 1996), Mentelle Basin (Petrizzo et al., 2021a, 2021b, 2022). In terms of data on benthic foraminifera, the balance is similar: the response to OAE 2 is well studied in the Northern Hemisphere (e.g., Schlanger and Jenkyns, 1976; Erbacher et al., 2005; Gebhardt, 2006; Jenkyns, 2010; Friedrich et al., 2006b, 2006a) and only sparse Southern Ocean records shed light on the benthic foraminiferal assemblages (i.e., Kerguelen Plateau: Holbourn and Kuhnt, 2002; Cauvery basin: Tewari et al., 1996; Western Australia, Haig et al., 2004).

The International Ocean Discovery Program (IODP) Expedition 369 Australia Cretaceous Climate and Tectonics recovered an almost complete pelagic record of the Upper Cretaceous, including the OAE 2 at Site U1516 in the Mentelle Basin, southeast Indian Ocean, offshore western Australia (Huber et al., 2019a). The present study at Site U1516 complements previous studies (Petrizzo et al., 2022, 2021a, 2021b) by focussing on the benthic foraminiferal record spanning the OAE 2.

2. Study area

Site U1516 is located offshore western Australia in the southeastern Indian Ocean. Expedition 369 drilled Holes U1516C (34°20.9272′ S, 112°47.9711′ E) and U1516D (34°20.9277′ S, 112°47.9573′ E) at 2676.6 m water depth in the Mentelle Basin on the eastern flank of the Naturaliste Plateau (Fig. 1). The Mentelle Basin and Naturaliste Plateau complex emerged during the breakup of East Gondwana and the ongoing divergence between Australia and Antarctica. The studied area was positioned at a triple junction between the Australian, Antarctic, and Indian plates. Rifting of eastern Gondwana started during the Middle Jurassic (Callovian) and led to an extension between India and Australia – Antarctica (e.g., Gaina et al., 2007; Direen et al., 2008; Gibbons et al., 2012; Harry et al., 2020; Lee et al., 2020). The next rifting phase during the Early Cretaceous led to further rifting and finally the breakup that started during the late Valanginian affecting the Cuvier and Perth Abyssal Plain (Huber et al., 2019a; Harry et al., 2020; Lee et al., 2020; Wainman et al., 2020; Wolfgring et al., 2021). In this phase, the Cretaceous sedimentary records documented at the Naturaliste Plateau and in the Mentelle Basin, were deposited in a thermally subsiding basin (White et al., 2013).

3. Methods

3.1. Biostratigraphic framework and geochemical data

Expedition 369 recovered a continuous Albian to Turonian sequence of sediments that is overlain by Paleocene to Pleistocene material at Site U1516 (Huber et al., 2019a). This study focuses on a ~19 m thick composite succession at Holes U1516C and U1516D from 459.72 to 478.50 m rCCSF (revised Composite Core depth below Sea Floor, LIMS online report portal at http://web.iodp.tamu.edu/LORE/, Huber et al., 2019b; Petrizzo et al., 2021a) spanning the Cenomanian–Turonian transition and the OAE 2 at Holes U1516C and U1516D (Fig. 2). Details on the drilling operations, logging, physical properties, magnetostratigraphy, geochemistry and sedimentology for Site U1516 are presented in the IODP Expedition 369 proceedings report (Huber et al., 2019a).

Site U1516 represents one of the few records of benthic foraminifera during the OAE 2 in the Southern Hemisphere. To document similarities and differences with other sections recording benthic communities in outer neritic to upper bathyal settings during the Cenomanian–Turonian transition, we compare biostratigraphic markers and variations in the abundance of taxa. Several globally recognized taxa recorded across the Cenomanian–Turonian transition and OAE 2 have been identified at Site U1516 and they correlate at species level to the records of neritic to upper bathyal settings in other localities. However, due to the scarcity and limited extent of the high latitudes record and to common taxonomic inconsistency, the correlation of benthic biostratigraphic data faces some setbacks and are sometimes limited to the genus level. The presumably epibenthic taxa, and particularly *Conorboides, Stensioeina*, *Gavelinella* (i.e., *G. vesca,* and *G. intermedia*) can be correlated to other low to high latitudes sections. Among infaunal taxa, the genera *Praebulimina* (e.g., *P. elata, P. nannina*), *Tappanina* and *Pleurostomella* (*P. subnodosa*) show a cosmopolitan distribution. Characteristic agglutinated taxa from the Cenomanian–Turonian transition at Site U1516 include *Clavulinoides gaultinus, Gaudryina pyramidata, Spiroplectinata annectens* and *Bulbobaculites.*

The biostratigraphic framework based on planktonic foraminiferal and calcareous nannofossil datums and the chemostratigraphic dataset (total organic carbon and bulk carbonate $\delta^{18}O$ and $\delta^{13}C$ measurements) are based on Petrizzo et al. (2021a, 2022). For details on lithostratigraphy and core data of Site U1516, we refer to Bogus et al. (2019) and Huber et al. (2019a). Petrizzo et al. (2021a) identified four intervals through the OAE 2 according to changes in the composition and abundance of the microfossil assemblages. In the present paper we identified those intervals (Fig. 2) as follows: pre OAE-interval (478.50 m–475.12 m rCCSF), pre max-CIE interval (474.38 m–471.12 m rCCSF), low $CaCO_3$ interval (470.36 m–467.96 m rCCSF), and post low $CaCO_3$ interval (467.72 m–459.72 m rCCSF).

We explore the benthic foraminiferal assemblage changes through the OAE 2 interval and compare developments in the assemblages to X-ray fluorescence (XRF) data. The XRF data presented herein was logarithmized to avoid the overestimation of peaks (Weltje and Tjallingii, 2008). The ratios of Fe/K and Fe/Zr, as well as the ratios of Ba/Ti and Ca/Ti are discussed as they represent

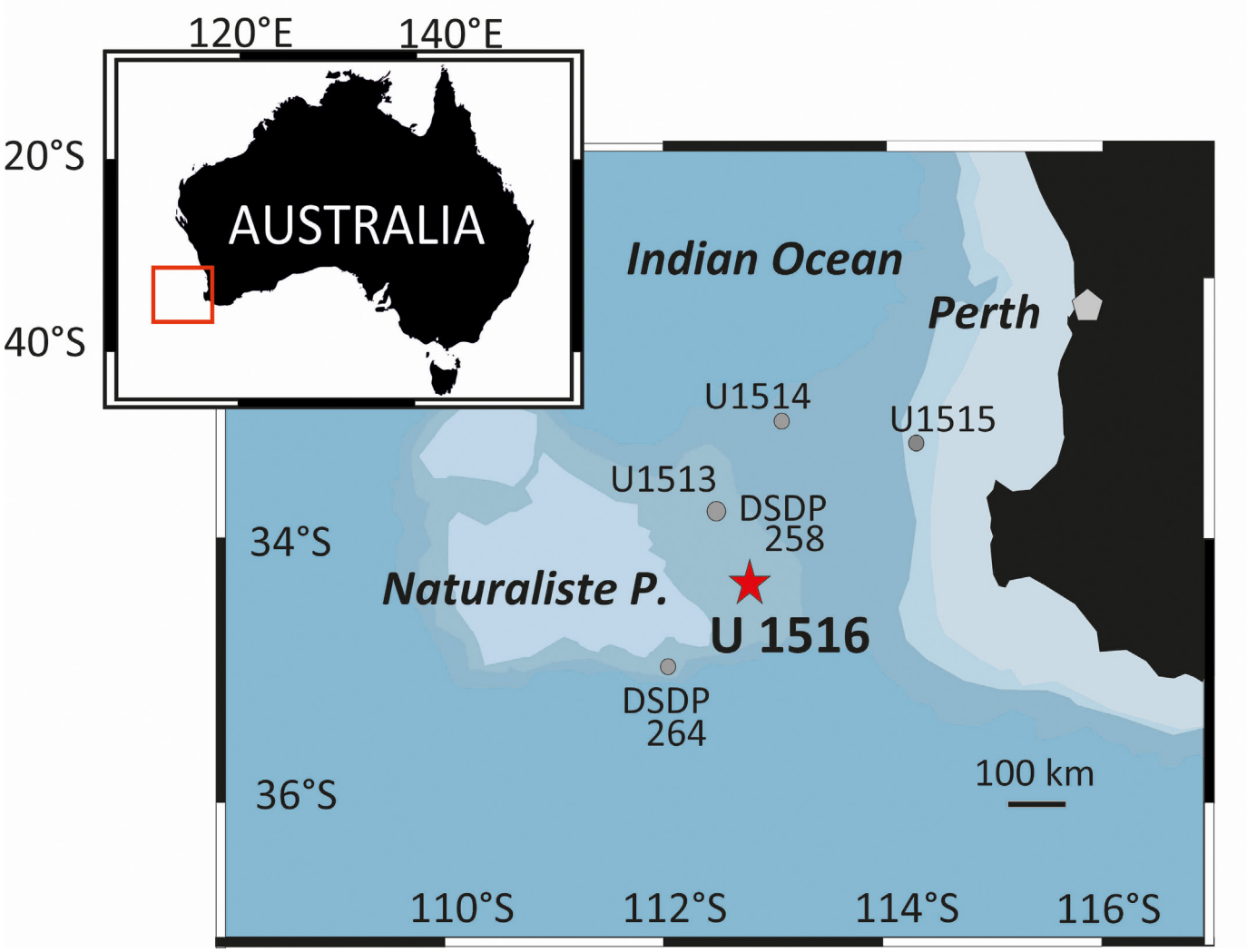

Fig. 1. Map of the studied area in the Mentelle basin (MB) on the eastern flank of the Naturaliste Plateau, offshore western Australia. IODP Site U1516 is denoted by a red star. Other sites drilled during IODP Expedition 369 and DSDP Site 264 are denoted by grey circles.

important paleoenvironmental proxies, that help to shed light on paleoproductivity and ocean chemistry (Fig. 2). The element Ba is understood as marker for surface and export productivity, and thus bioproduction and food supply (Klump et al., 2000; Croudace and Rothwell, 2015). Barium is removed from the water column in the euphotic zone (in organic matter production). The Ba content depends on the flux and sedimentation of Ba in particulate organic matter and is positively influenced by warmer water-temperatures (Carter et al., 2020; Lowery and Bralower, 2022). However, most Ba is sourced from runoff and weathering and additionally hydrothermal effluents (e.g., Carter et al., 2020; Dickens et al., 2003; Klump et al., 2000). As variations in the Ba content frequently depend on changes in terrigenous sources, we normalize elemental Ba against Ti to make up for detrital influence from runoff (as discussed in detail in Lowery and Bralower, 2022 and Hull and Norris, 2011).

The elemental concentration of Ca provides important indications to the understanding of developments in biogenic carbonate productivity. Calcite saturation or dissolution due to varying levels of acidification and alkalinity, are among the most important parameters used to interpret assemblages and closely linked to the latter proxies (Sliter, 1975; Gebhardt, 2006; Gebhardt et al., 2008; Nguyen et al., 2009; Croudace and Rothwell, 2015).

The elemental proportion of Fe in marine sediments represents an important proxy for terrigenous input and continental runoff (Haug et al., 2001; Bertrand et al., 2015). The Fe/K and Fe/Zr ratios are both considered sensible to local climatic variability: the Fe/K ratios were used to follow changes in precipitation and runoff, provenance, and associated clay mineralogy. The elemental K-content correlates to the amount of the clay mineral Illite. An increase in the proportion of the latter can be interpreted as increased precipitation and humidity. The interpretation of changes in the Fe/K ratio as indicators for changing palaeoclimatic characteristics regarding material from humid, vs. weathered material from dryer regions has been documented in e.g., Govin et al. (2012), Chen et al. (2022).

Similarly, the Fe/Zr ratios can indicate changes in provenance and catchment area, and runoff. Variations in the share of the heavier Zr associated to Fe could illustrate changing sources and nature of terrigenous runoff to the basin. This ratio can be understood as proxy to identify changes in weathering and runoff as low Fe/Zr values represent an enrichment in the heavier element Zr and can thus be linked to times of low weathering and arid conditions (Hanebuth and Lantzsch, 2008; Croudace and Rothwell, 2015; Neuhuber et al., 2016; Corentin et al., 2020; Chen et al., 2023, 2022).

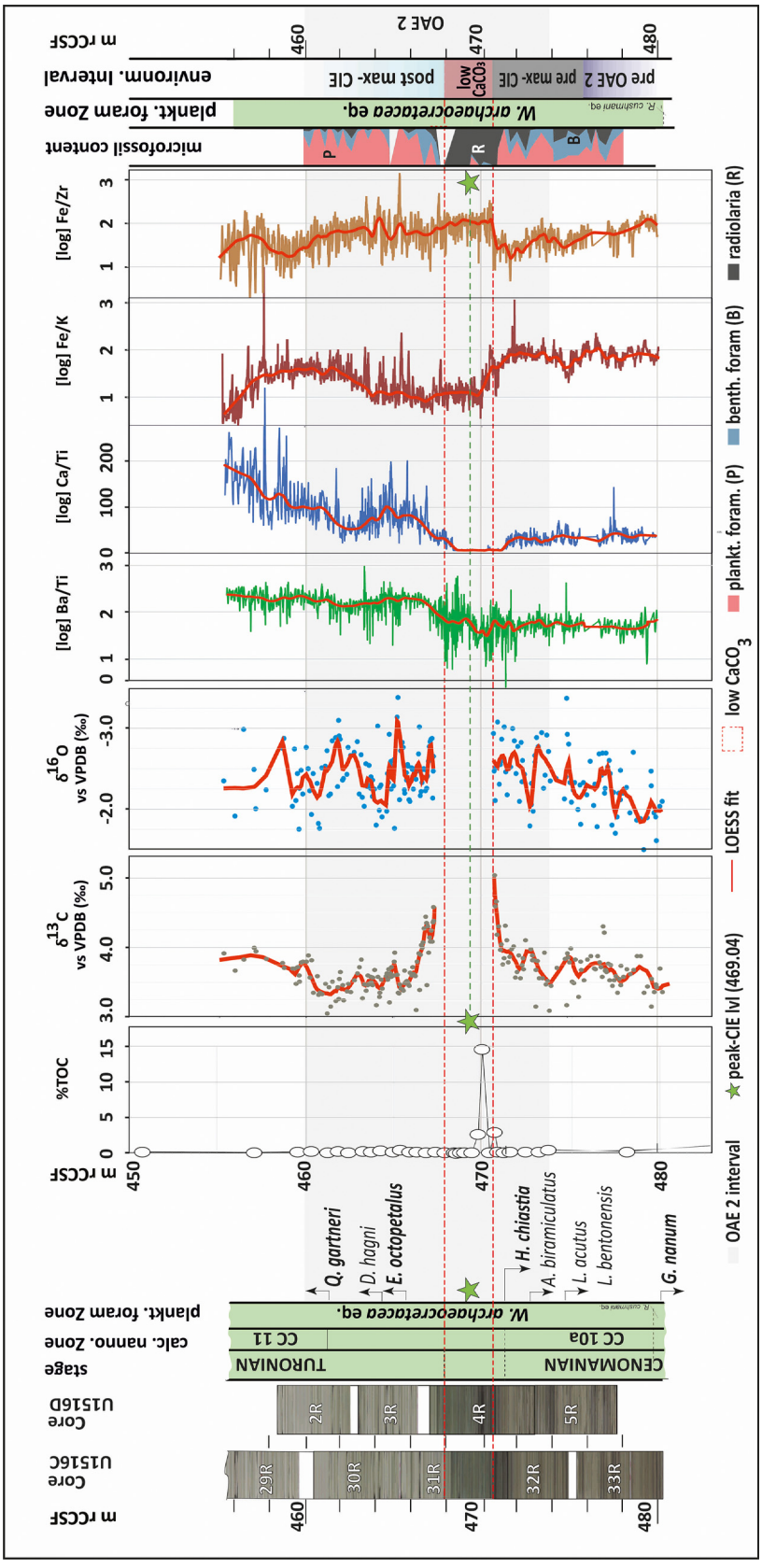

Fig. 2. Core recovery and stratigraphic framework of the Cenomanian–Turonian transition at Site U1516. Lithostratigraphy and core recovery after Huber et al. (2019a). Bio and chronostratigraphy, Total Organic Carbon (TOC), δ13C and δ18O measurements, OAE 2 interval (grey), max CIE – level (marked by green star), LOESS fit = 0.04, microfossil content and environmental intervals after Petrizzo et al. (2021a, 2022) and this study. XRF (X-ray fluorescence) signature of log XRF ratios of Ba/Ti, Ca/Ti, Fe/K and Fe/Zr from Bogus et al. (2019).

3.2. Foraminiferal methods

We focus on benthic foraminiferal assemblages from 32 samples that were examined for planktonic foraminifera and calcareous nannofossils in a previous study (Petrizzo et al., 2022, 2021a,b). Samples of 30 cm^3 were weighed, soaked in a solution of H_2O_2 and water, washed over >38, >125 and > 250 μm sieves and dried. The resulting residues were picked, and microfossils placed on microslides. If not stated otherwise in the text, the density or standing crop of benthicand planktonic foraminifera and of radiolaria is given as number of individuals per gram of dry sediment (i.e., BF/g: Benthic Foraminifera/gram, see Murray and Alve, 2000). Benthic foraminifera recovered in the small size fraction (38–125 μm) were not identified at the genus/species level because taxonomically important features could not be confidently observed on most individuals. Foraminiferal microslides are stored in the Micropalaeontology Collection at the Dipartimento di Scienze della Terra "A. Desio", Università degli Studi di Milano. The benthic foraminiferal taxonomy generally follows Holbourn and Kuhnt (2002) that discusses benthic foraminiferal assemblages from comparable environmental settings.

Oxygen saturation related terminology refers to Wignall et al. (2010) (i.e., in descending order of oxygen content: oxic, dysoxic and suboxic). Paleodepth categorizations follows Nyong and Olsson (1984): neritic 0–200 m (i.e., inner – 0–50 m, middle – 50–100 m and outer-neritic – 100–200 m), bathyal 200–2500 m (i.e., upper – 200–500 m, middle – 500–1500 m and lower-bathyal – 1500–2500 m) and abyssal >2500 m.

Recent analogues as well as palaeoecologic interpretations of foraminiferal taxa outlined in Alegret et al. (2009); Bernhard (1986); Friedrich et al. (2006a); Friedrich and Hemleben (2007); Jorissen et al. (2007); Kaiho (1994); Kaiho et al. (2006); Wendler et al. (2013) are used to interpret the possible habitat preferences (infaunal/epibenthic, oxic/dysoxic/anoxic).

Corroborating the possible interpretations on the palecology of benthic foraminifera, a foraminiferal morphogroup analysis linking test morphologies to habitat preferences and feeding strategies is presented. For better understanding of benthic foraminiferal morphogroups, we follow schemes that integrated the works of Corliss (1985), Jones and Charnock (1985), Kaminski et al. (1995) and Murray et al. (2011). The morphogroup scheme applied for calcareous species is based on Koutsoukos and Hart (1990) analysing benthic foraminiferal distributions through the Cenomanian/Turonian of the Sergipe Basin, Brazil, and Frenzel (2000) on benthic foraminifera of the Maastrichtian of Rügen, Germany that integrated studies based on the distribution of modern foraminiferal taxa originally applied in Jones and Charnock (1985) and modified in Bernhard (1986) and Corliss and Chen (1988). Agglutinated foraminifera were categorized according to the morphogroup scheme applied in Setoyama et al. (2017), which is based on Jones and Charnock (1985) and modifications by (Bąk et al., 1997; Peryt et al., 2004 and Cetean et al., 2011).

Foraminiferal morphogroups established for calcareous and agglutinated benthic foraminifera are presented in Table 1. The classification of morphotypes considered 13 types, divided into two subgroups, of calcareous hyaline (CH-A 1–8 and CH-B 1–5)– , calcareous porcelaneous (CP) – and 4 agglutinated foraminiferal morphotypes (M1–4) (Table 1). Taxa with planoconvex or low trochospiral chamber arrangement recorded at Site U1516, i.e., the epibenthic taxa *Gavelinella, Conorboides,* and *Stensioeina,* supposedly thrived on the ocean floor or in the uppermost layers of sediment (morphogroups CH-A 1, 2 and 5). Some members of this group (mostly gavelinellids) are suspected to tolerate dysoxic conditions in eutrophic settings (Holbourn and Kuhnt, 2002; Friedrich et al., 2006b; Friedrich, 2010).

Calcareous benthic species with an epi- to infaunal habitat preference can be found in morphogroups CH-A 3, 4 and 6. The morphologic characteristics of *Lingulogavelinella frankei* and *L. turonica* are found in group CH-A 3 and suggest an epi-to infaunal habitat preference. *Gyroidinoides* spp. are considered opportunistic to generalistic taxa that presumably occupied epibenthic to deep infaunal habitats and tolerated sub- and dysoxic conditions (Alegret et al., 2003; Friedrich et al., 2006b; Jorissen et al., 2007; Reolid et al., 2012; Wolfgring et al., 2022), thus indicating, like coiled vaginulids (*Lentuculina* spp., *Astacolus* spp.), unclear habitat preferences in morphogroups CH-A 4 and CH-A 6.

The dominant taxa in morphogroup CH-B 1 are *Pleurostomella, Lagena* and *Pyrulina* are all reconstructed to tolerate suboxic to dysoxic habitats, while the dominant taxon in CH-B 2, *Frondicularia* sp. is considered to prefer oxic habitats (Alegret et al., 2003). The *Dentalina/Nodosaria* group can be found in CH-B 3**,** which predominantly represents forms that tolerate poorly oxygenated habitats (e.g., Kaiho, 1994; Alegret et al., 2003; Reolid et al., 2012). The remainder in the calcareous benthic group can be found in CH-B 4, dominated by *Praebulimina,* and CH-B 5 represented by a single occurrence of *Tappanina.* The occurrence in either group suggest an infaunal habitat in eutrophic environments.

Few agglutinated foraminiferal species were recorded in the investigated interval: the low oxygen tolerant, infaunal taxa *Spiroplectinata* and *Spiroplectammina* (dominating the agglutinated morphogroup M2-c), *Glomospira charoides* (representing M3-a) and the more frequently observed *Clavulinoides gaultinus* (dominant in morphogroup M3-a) are to be mentioned. A benthic foraminiferal taxonomic reference list and species counts together with remarks on ecology and benthic foraminiferal morphogroups are provided in the supplementary materials (Supplementary materials S1, ST1) and the online repository PANGAEA in (Wolfgring et al., 2023).

3.3. Statistical methods

Benthic foraminiferal abundance data of Site U1516 (proportions of individuals per taxon/sample) were subjected to hierarchical clustering and Correspondence Analysis. The programmes Past (Hammer et al., 2001) and the "stats" package written in the language R were applied (R Core Team, 2022). To reduce noise in multivariate analysis and improve the significance of environmental interpretations, the dataset was reduced to taxa representing more than 0.5% of the total benthic foraminiferal dataset, covering 82.44% of all data assessed in this study.

We conducted a hierarchical clustering after Ward (1963) (requiring Euclidean distances), to explore similarities in the taxonomic composition of benthic foraminiferal assemblages per sample. The results of this method can be further supported and validated by a Detrended Correspondence Analysis (DCA, Hill and Gauch, 1980; Oxanen and Minchin, 1997) to explore relations between samples according to variance in relative abundance data and to identify variables indicative of shifts in foraminiferal paleoenvironments. To eliminate outliers and overestimation of single datapoints during multivariate analysis, proportional data per sample was row-normalized (dividing all values through the Euclidean norm of the respective row, i.e., the taxon counts per sample). For detailed results of the cluster analysis and column scores of the DCA see Supplementary materials Tables ST2 and ST3.

The Shannon diversity index (H) (Shannon and Weaver, 1949) and Dominance (D) (Simpson, 1949) were calculated. Shannon (H)

Table 1
Morphotype categories of benthic foraminifera (modified after Koutsoukos and Hart, 1990 for calcareous- and Setoyama et al., 2017 for agglutinated foraminifera). CH = calcareous hyaline, CP = calcareous porcelaneous, M = agglutinated morphotype.

CH-A	1	Plano-convex, low/high trochospiral, broad	Epifaunal	Deposit feeders	Neritic – upper bathyal	Planoconvex high trochospiral (e.g., *Gavelinella intermedia, Conorboides claytonensis*)
	2	Concavo-convex, low trochospiral, broad	Epifaunal	Deposit feeders	Neritic – upper bathyal	Low trochospiral, compressed, asymmetrical planoconvex to concavoconvex tests (e.g., *Gavelinella cenomanica, Stensioeina* sp.)
	3	Inflated biconvex, periphery broadly rounded	Epifaunal/infaunal	Deposit feeders	Outer neritic – upper bathyal	Biconvex, broad, rounded periphery (e.g., *Lingulogavelinella frankei, L. turonica*)
	4	Conical, low trochospiral	Epifaunal/infaunal	Deposit feeders and passive herbivores	Middle neritic – upper bathyal	Low trochospiral, flattened spiral and convex umbilical side (e.g., *Gyroidinoides* spp.)
	5	Lenticular, low trochospiral periphery subacute/carinate	Epifaunal	Deposit feeders	Middle neritic – upper bathyal	Low trochospiral, nearly planispiral (*Notoplanulina compressa*)
	6	Lenticular, planispiral periphery, subacute/ carinate	Epifaunal/infaunal	Deposit feeders	Neritic – upper/middle bathyal	Coiled vaginulids (e.g., *Lentuculina* spp., *Astacolus* sp.)
	7	Conical, low/high trochospiral	Epifaunal	Deposit feeders and passive herbivores	Neritic	–
	8	Discoidal-flattened	Bilocular	Deposit feeders	Neritic	–
CH-B	1	Globular/ovate to elongate/fusiform	Epifaunal/infaunal	Deposit feeders	Neritic – upper/middle bathyal	Globular to ovate morphotypes, low trochospiral to triserial uniserial test elongate (e.g., *Pleurostomella* spp., *Lagena* sp., *Pyrulina* sp.)
	2	Broad to palmate, compressed planispiral to uncoiled uniserial	Epifaunal/infaunal	Deposit feeders	Neritic – upper bathyal	Flattened planispiral to uniserial (e.g., *Frondicularia* sp.)
	3	Elongate, straight to arcuate uniserial or planispiral-uniserial	Epifaunal/infaunal	Deposit feeders	Neritic – upper/middle bathyal	Elongate straight (e.g., *Nodosaria/Dentalina*)
	4	Tapered rounded elongate triserial, biserial, uniserial	Infaunal	Deposit feeders	Middle/outer neritic – upper/middle bathyal	Tapered, rounded-elongate bi-, triserial (e.g., *Praebulimina* sp.)
	5	Tapered flattened-elongate biserial	Infaunal	Deposit feeders	Middle/outer neritic – upper/middle bathyal	Flattened elongate compressed (*Tappanina* sp.)
CP (A,B)	CP	Porcelaneous walled	Epifaunal/shallow infaunal	Suspension feeders	Middle to outer neritic – upper bathyal	–
M1	M1-a	Tubular	Infaunal	Suspension feeding	Tranquil bathyal – abyssal	Tubular (*Bathysiphon* sp)
M2	M2-a	Globular	Shallow infauna	Suspension feeders and/or Passive deposit feeders	Bathyal – abyssal	–
	M2-b	Rounded trochospiral and steptospiral Planoconvex trochospiral	Epifaunal	Active deposit feeders	Shelf to deep marine	–
	M2-c	Elongate keeled	Epifaunal	Active deposit feeders	Neritic to marginal marine	Elongate keeled (*Spiroplectammina* sp., *Spiroplectinata* sp.)
M3	M3-a	Flattened trochospiral Flattened planispiral and streptospiral	Epifaunal	Active and passive deposit feeders	Lagoonal to abyssal	Flattened planispiral, streptospiral (e.g., *Glomospira charoides*)
	M3-b	Flattened irregular	Epifaunal	Suspension feeders	Upper bathyal – abyssal	–
	M3-c	Flattened streptospiral		Active and passive deposit feeders	Upper bathyal – abyssal	–
M4	M4-a	Rounded planispiral	Epifaunal/shallow infaunal	Active deposit feeders	Inner shelf – upper batyal	–
	M4-b	Elongate subcylindrical, elongate tapered	Deep infaunal	Active deposit feeders	Inner shelf – upper bathyal (with increased organic matter flux)	Elongate subcylindrical (e.g., *Clavulinoides gaultinus*)

considers the number of species and the relative abundance of individuals per taxon in a sample to quantify changes in diversity. The minimum value is 0 when only one taxon can be recorded. The Dominance index (D) ranges from 0 to 1, where 0 indicates a community with all taxa equally present, and 1 is the maximum value indicating a single taxon present, thus dominating the assemblage.

4. Results

4.1. Composition of microfossil assemblages

Microfossil assemblages recovered at the Cenomanian–Turonian transition at Site U1516 (478.50–459.72 m rCCSF) are generally dominated by calcareous microfossils (Fig. 3).

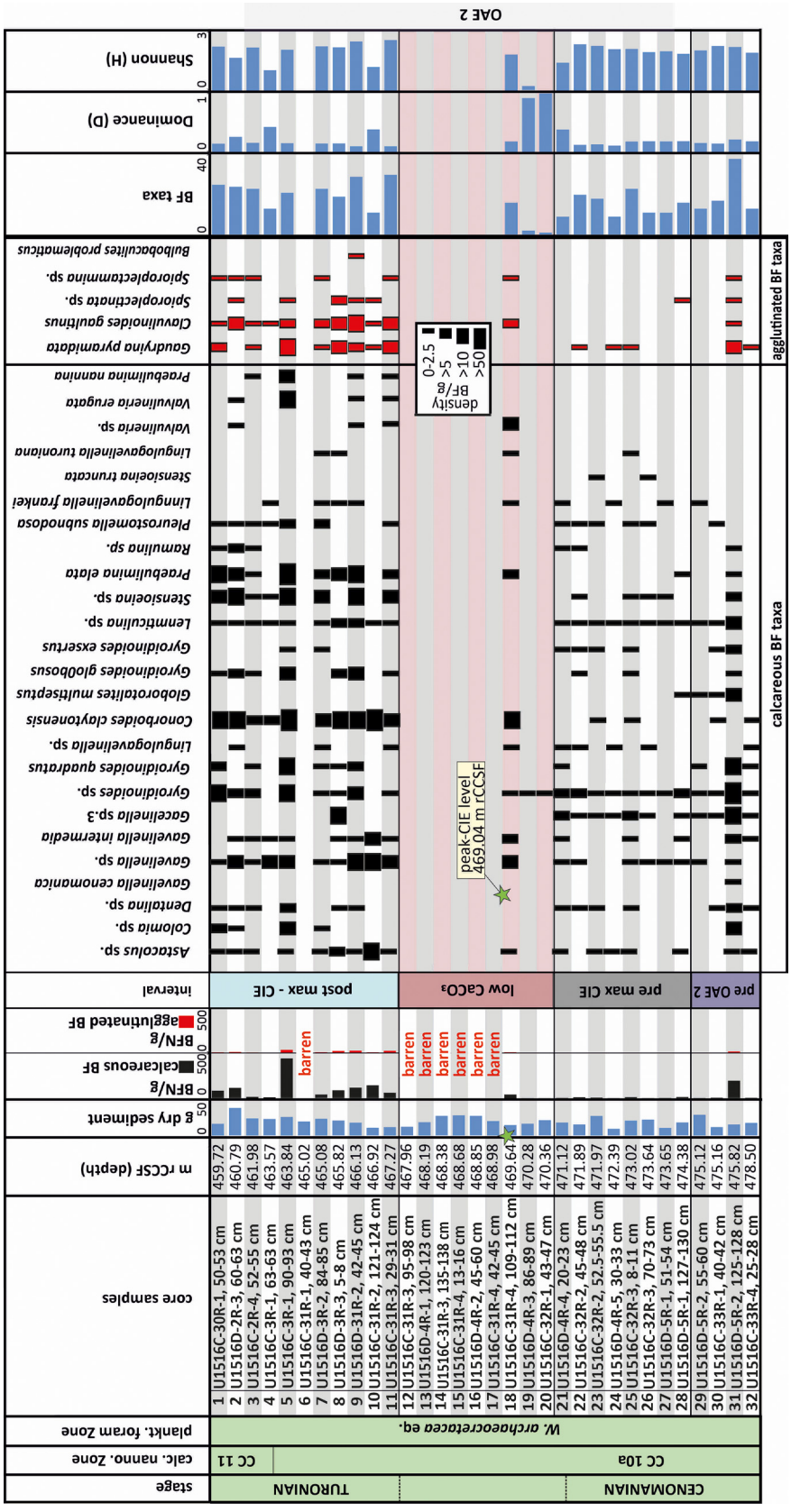

Fig. 3. Density (individuals per gram of dry sediment) of benthic foraminiferal taxa (black = calcareous taxa, red = agglutinated taxa) with either a share of more than 0.5 percent of the total benthic foraminiferal assemblage (>125 μm), or of biostratigraphic significance, together with Shannon (H) and Dominance (D) index values. Biostratigraphic framework and intervals according to Petrizzo et al. (2021a, 2022). Environmental interval according to this study. BF/g = Benthic foraminifera per gram of dry sediment.

Radiolaria become the dominant microfossils during the low $CaCO_3$ interval between 470.36 m rCCSF and 467.96 m rCCSF. Below and above this interval, planktonic foraminifera dominate the assemblage (Petrizzo et al., 2021a). Benthic foraminifera are only absent between 486.98 m rCCSF and 467.96 m rCCSF in the low $CaCO_3$ interval and in a sample at 465.02 m rCCSF. Benthic foraminiferal preservation below the low $CaCO_3$ interval was perceived as moderate, whereas ranges from good to excellent in the overlying interval.

Benthic foraminifera illustrate outer neritic to upper bathyal depth distributions. We base our paleodepth estimate for Site U1516on bathymetric ranges of Cenomanian-Turonian benthic foraminiferal taxa and assemblages, i.e., Gebhardt (2006); Howe et al. (2000), Kaminski et al. (1999), Koutsoukos and Hart (1990), Koutsoukos (1989), Sikora and Olsson (1991) (see Supplementary material 1: Taxonomic reference list for depth ranges of significant taxa) and the typical bathymetric distribution of benthic foraminiferal morphotypes recovered (see Table 1).

4.2. Benthic foraminiferal assemblage data

The benthic foraminiferal assemblage is composed by 71 species and 34 genera. Fig. 3 shows the benthic foraminiferal density per gram of dry sediment of taxa that exceed 1% of the total benthic assemblage, whereas Fig. 4 illustrates the relative abundance of benthic foraminiferal ecologic groups and genera as well as representative species. Significant benthic foraminiferal taxa are illustrated in Figs. 5 and 6. Calcareous foraminifera prevail throughout, agglutinated taxa are rare between 478.50 m rCCSF and 469.64 m rCCSF and increase in abundance between 467.27 m rCCSF and 459.72 m rCCSF. Through the different intervals, we observe high fluctuations in the density of benthic foraminifera (BF/g) and number of taxa as well as in the Dominance (D) and Shannon (H) indices (Fig. 3). Associated changes in the Ba/Ti and Ca/Ti signatures (Fig. 4) help to interpret paleoenvironmental conditions such as paleoproductivity and redox conditions. The following Intervals (Figs. 3, 4) already identified in Petrizzo et al. (2021a) are analysed regarding the changes in benthic foraminiferal data, as follows.

1) pre-OAE 2 Interval (478.50–475.12 m rCCSF)

The benthic foraminiferal density fluctuates between 2 and 5 specimens per gram of dry sediment (BF/g) with one exception of ~180 BF/g at 475.82 m rCCSF. The four samples investigated in this interval (Figs. 3, 4) show an unevenly distributed taxa richness. Sample 475.82 m rCCSF yields the highest taxon diversity with 38 taxa, while the other samples record significantly less taxa (13–17). This is likewise reflected in the Shannon (H) and Dominance (D) indices of 2–2.3 and 0.15–2, respectively. The benthic taxa *Gavelinella* sp. 3, *Globorotalites multiseptus*, *Gyroidinoides quadratus*, *Gyroidinoides* sp., and *Lenticulina* spp. are abundant in this interval (dominant morpohgroups CH-A2 and CH-A4). Agglutinated taxa (i.e., *Gaudryina pyramidata, Clavulinoides gaultinus* and *Spiroplectinata* sp., morphogroups M2-c and M4-b) are present from above 478.50 m rCCSF. *Gavelinella cenomanica* only appears in this interval. The taxa *Gavelinella* sp. 3 and *Gyroidinoides* sp. represent ~30% of the benthic assemblage each (Fig. 4). The lowermost samples contain oxic taxa (i.e., *Globorotalites* sp.) and eutrophic taxa (i.e., *Praebulimin*a sp.) that are a minor component. The pre-OAE interval records comparatively low values in [log]Ba/Ti and [log]Ca/Ti (Figs. 2, 4): the [log]Ba/Ti signature presents a very slight positive trend through the base of the section fluctuating between [log]Ba/Ti = 1.5 and 1.8. The [log]Ca/Ti curve depicts a marginally decreasing pattern from [log]Ca/Ti = ~30 to [log]Ca/Ti = ~20 interrupted by a short excursion to [log]Ca/Ti = ~120 at ~478 m rCCSF.

2) pre-max CIE – Interval, 474.38 m rCCSF – 471.12 m rCCSF:

The pre-max CIE interval (Figs. 3 and 4) illustrates a depauperate assemblage (mostly less than 5 BF/g per sample between ~470 and 480 m rCCSF) dominated by *Gyroidinoides* spp. and *Gavelinella* spp. that compose more than the 50% of the assemblage in some samples. Furthermore, the calcareous taxa *Gavelinella* sp. 3, *Gavelinella* sp., *Gyroidinoides* sp. and *Lenticulina gibba* are abundant and present in low numbers (less than 5 BF/g). The benthic foraminifera *Stensioeina truncata* is only recorded in this interval, whereas the epifaunal *Globorotalites multiseptus* is absent. The most abundant taxa are *Gavelinella* sp. 3 and *Gyroidinoides* sp., showing almost the same relative abundance as in the preceding interval (~25% and ~22%). Agglutinated foraminifera were only recorded in 50% of the samples: *Gaudryina pyramidata* occurs at 473.38 m rCCSF, 471.97 m rCCSF and 471.89 m rCCSF, *Spiroplectinata* sp. occurs at 474.38 m rCCSF and *Clavulinoides gaultinus* was not documented in this Interval. Fig. 4 illustrates a slight shift in dominant foraminiferal morphogroups: morphogroups CH-A2 (dominated by *Gavelinella, Stensioeina*) and CH-A4 (predominantly *Gyroidinhoides*) still dominate the assemblage and we document an increase in CH-A6 and CH-B1, represented by e.g.: *Lenticulina* and *Pleurostomella,* respectively.

In general, the low total abundance of benthic foraminifera, the virtual absence of agglutinated taxa in most samples (between 0 and 6%), and the relatively high share of resilient taxa tolerant of reduced oxygen environments like *Gyroidinoides* or *Lenticulina,* indicate a mesotrophic setting in the pre-max CIE interval. Furthermore, the latter taxa are believed to display a broad environmental distribution and were documented from epibenthic to infaunal habitats (i.e., Alegret et al., 2003; Bernhard, 1986; Friedrich et al., 2006a; Friedrich and Hemleben, 2007; Gross, 2000; Jorissen et al., 2007; Kaiho, 1994; Kaiho et al., 2006; Tyszka, 1994; Wendler et al., 2013; Wolfgring et al., 2022).

The absolute abundance of benthic foraminifera illustrates a cyclic declining trend (Fig. 3). In average, this interval registers ~6 BF specimens/g, Shannon (H) and Dominance (D) indices between 474.38 m rCCSF and 471.90 m rCCSF show a slight increase and indicate an assemblage structure similar to the underlying pre OAE 2 interval. A change can be observed by a significant decline of Shannon (H) (1.49) and increase in Dominance (D) to ~0.4 in sample 471.12 m rCCSF. The pre-OAE 2 interval records a slight increase in [log]Ba/Ti suggesting elevated paleoproductivity (from [log]Ba/Ti = 1.7 to [log]Ba/Ti = 2 to ~100‰). The Ca curve depicts a cyclically decreasing pattern and fluctuates between [log]Ca/Ti = ~30 towards almost zero at the top of the pre max-CIE interval (Figs. 2, 4).

3) low $CaCO_3$ interval, 470.36 m rCCSF – 467.96 m rCCSF

Encompassing the maximum Carbon Isotope Excursion (max CIE) with peak value at 469.04 m rCCSF (Petrizzo et al., 2021a), the low $CaCO_3$ interval (Figs. 2, 3) is characterized by highly abundant radiolaria and a depauperate benthic assemblage between 467.27 m rCCSF and 466.92 m rCCSF (0.04 and 1.3 individuals of *Gyroidinoides* sp. per gram of dry sediment), followed by a sample with comparatively high density of benthic foraminifera (sample at 469.64 m rCCSF that yields 40.7 BF/g), and subsequently followed by a barren interval between 468.98 m rCCSF and 467.96 m rCCSF.

The first two samples of this interval show high values in Dominance (D) that are mirrored in low values in the Shannon index (H). The sample with the highest abundance of benthic foraminifera in the low $CaCO_3$ interval at 469.64 m rCCSF (sample

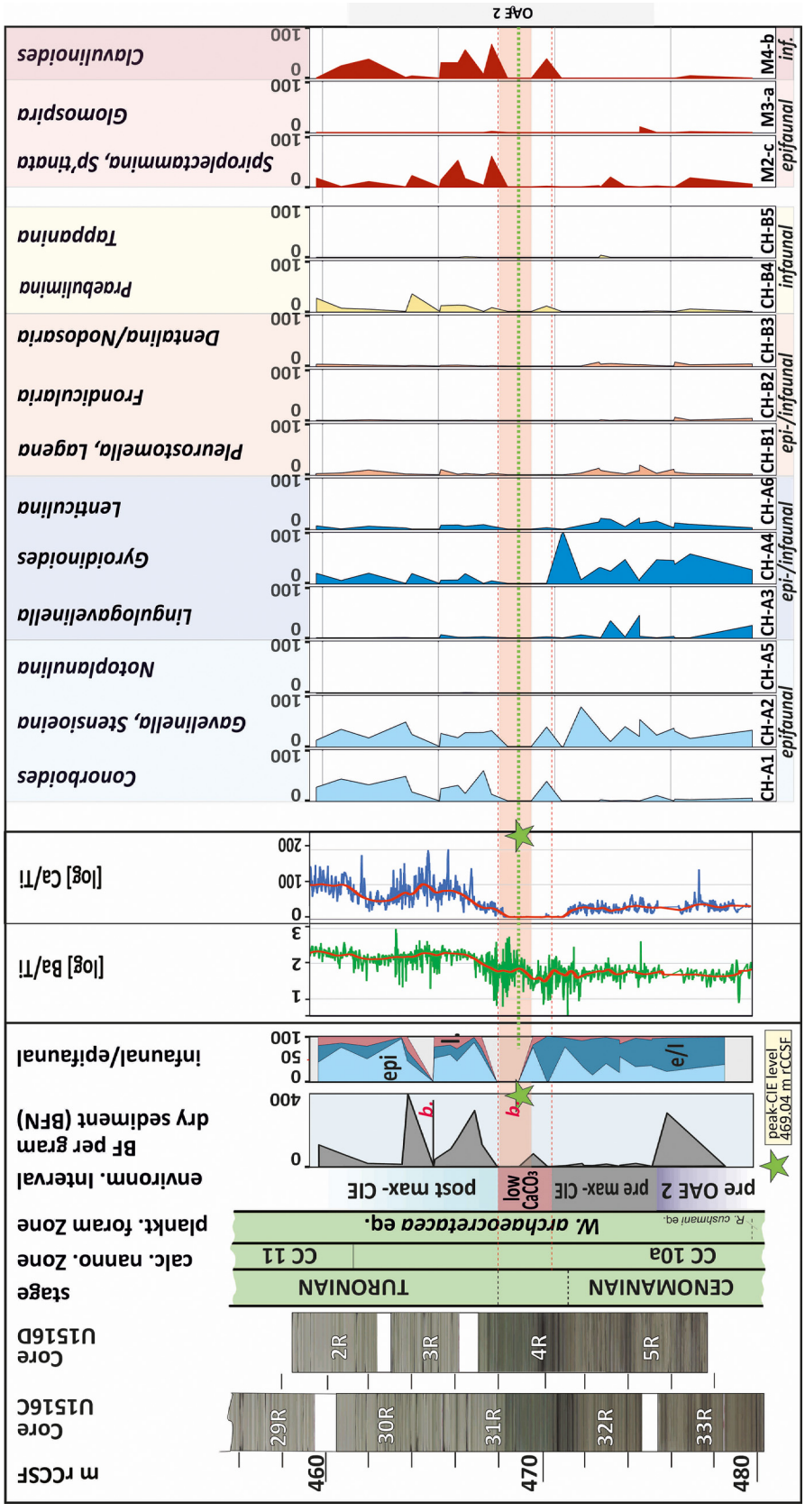

Fig. 4. Relative abundance of morphogroups in benthic foraminifera by habitat preference (epi = epifaunal benthic taxa, in = infaunal benthic taxa, in/epi = taxa with unclear habitat preference). Relative abundance of benthic foraminiferal morphogroups and respective dominant species therein. Ratios of [log]Ca/Ti and [log]Ba/Ti, Biostratigraphic framework and intervals according to Petrizzo et al. (2021a, 2022); eq. = equivalent. Environmental intervals according to this study. BF/g = density of benthic foraminifera per gram of dry sediment (>125 μm), b. = barren samples. Spiroplectinata = Sp'tinata.

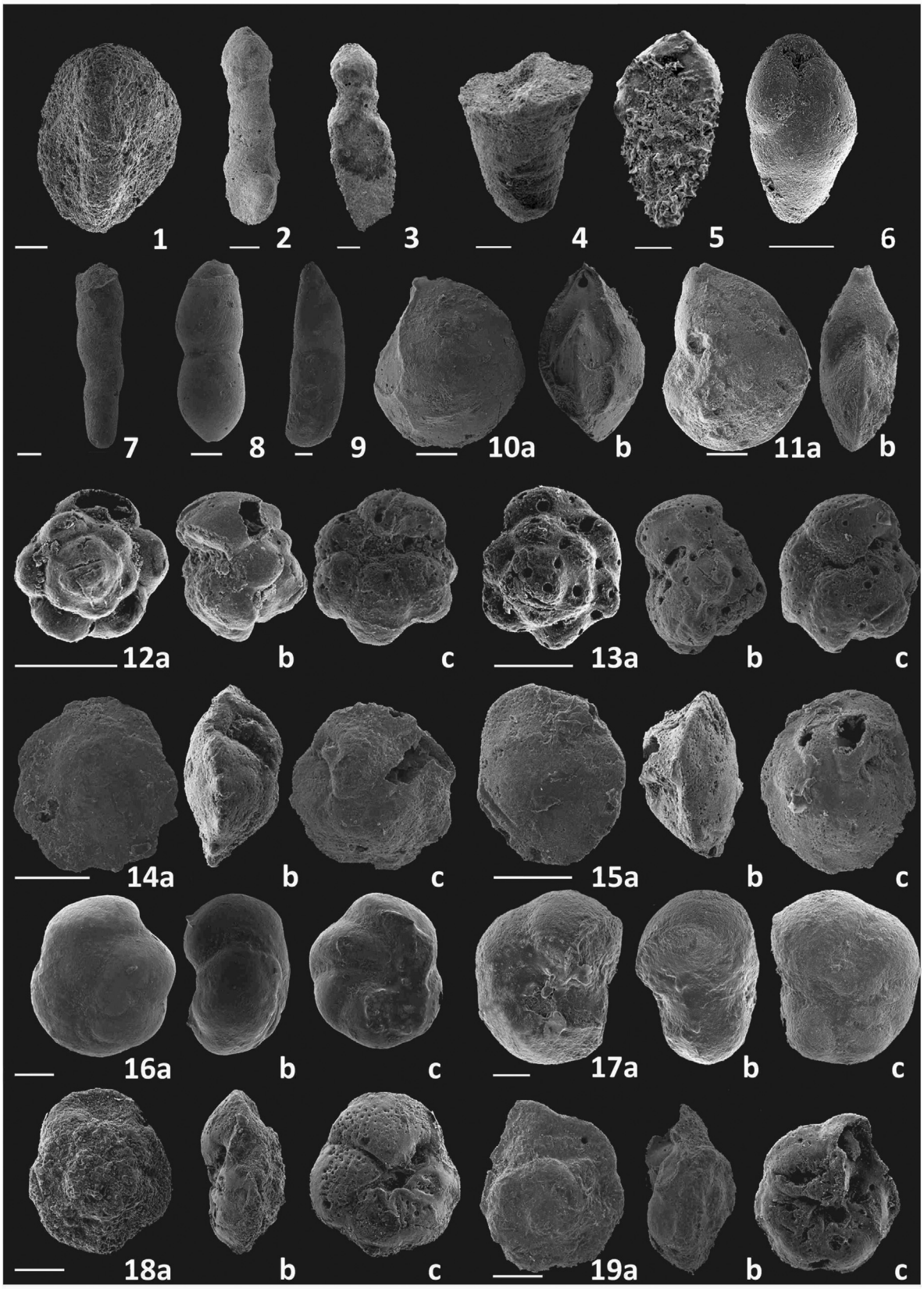

Fig. 5. SEM images of selected benthic foraminifera from Site U1516. 1) *Gaudryina pyramidata*, U1516C-33R-4, 25–28 cm; 2) *Clavulinoides gaultinus*, U1516D-2R-3, 60–63 cm; 3) *Spiroplectinata annectens*, U1516D-5R-2, 125–128 cm; 4) *Colomia* sp. (?), U1516D-5R-2, 125–128 cm 28 cm; 5) *Tappanina* sp., U1516D-2R-2, 125–128 cm; 6) *Praebulimina elata*, U1516D-3R-1, 90–93 cm; 7) *Pleurostomella subnodosa*, U1516D-2R-3, 60–63 cm; 8) *Dentalina* sp., U1516D-5R-1, 127–130 cm; 9) *Dentalina cylindroides*, U1516D-2R-3, 60–63 cm; 10a, b) *Lenticulina muensteri*, U1516D-5R-2, 125–128 cm; 11a,b) *Lenticulina* sp. cf. *L. gibba*, U1516D-5R-2, 125–128 cm; 12a, b, c); *Gyroidinoides quadratus*, U1516C-33R-4, 25–28 cm; 13a,

U1516C-31R-4, 109–112 cm) shows values for Dominance (D) and Shannon (H) indices of 0.18 and 1.9, respectively. In this sample we record a benthic foraminiferal assemblage with a distinctly different composition compared to the preceding interval below 470.36 m rCCSF. The recurrence of agglutinated taxa (i.e., *Clavulinoides gaultinus*, *Spiroplectammina* sp.) coincides with the recurrence of calcareous taxa, particularly gavelinellids (*Gavelinella intermedia* and *Gavelinella* sp), *Conorboides claytonensis* and *Praebulimina* spp. The first two samples show high Dominance of *Gyroidinoides* sp., the sample at 469.64 m rCCSF records a high share of *Conorboides claytonensis* (~30%) and the 20% of the taxa are represented by *Gavelinella* and *Valvulineria* (Figs. 3, 4). Therefore, the low $CaCO_3$ interval is dominated by epifaunal morphogroups CH-A1 (e.g.: *Conorboides claytonensis*), CH-A2 (e.g.: *Gavelinella, Stensioeina*) and the epifaunal/infaunal CH-B3 (*Praebulimina*) as well as the presumably infaunal morphogroup M4-b (*Clavulinoides)*.

A bimodal pattern in the [log]Ba/Ti curve is documented with a first peak [log]Ba/Ti = ~2.2 between 470.20 and 469.50 m rCCSF, a short decline to [log]Ba/Ti = ~1.5 correlated to a barren interval, and a second excursion to [log]Ba/Ti = ~2.8 through ~ 469 m rCCSF and 468 m rCCSF. The highest abundance and the most diversified foraminifera within the low $CaCO_3$ interval can be found in sample U1516C 31R 4, 109–112 cm (469.64 m rCCSF). During the low $CaCO_3$ interval, the [log]Ca/Ti curve fluctuates from 0 to 1 between 470.60 m rCCSF and 467.40 m rCCSF (Figs. 2, 4). Both, [log]Fe/K and [log]Fe/Zr ratios show prominent changes at the base and through the low $CaCO_3$ interval. The [log]Fe/K curve illustrates a gradual decline from [log]Fe/K = 2 to [log]Fe/K = 1, while the [log]Fe/Zr curve shows an increase of the ratio from 1 to 2 (Fig. 2).

4) post max-CIE interval, 467.27 m rCCSF – 459.72 m rCCSF

Above 467.96 m rCCSF, benthic foraminiferal density and diversity increase and are represented by a strong increase in agglutinated as well as calcareous taxa averaging 103 BF/g per sample (Fig. 3). The calcareous assemblage is dominated by *Praebulimina* (~10%) and gavelinellids and osangularids (~45%). The latter group exhibits a continuously high taxonomic diversity and records the dominant *Gavelinella intermedia, Gavelinella* sp. and *Conorboides claytonensis,* abundant *Stensioeina* sp. and *Lingulogavelinella.* The most abundant taxa in this interval are *Conorboides claytonensis* (~30%), *Gavelinella* sp. (~12%), and *Stensioeina* sp. (~10%) (morphogroups CH-A1 and CH-A2). The marked increase in abundance of agglutinated taxa is illustrated in the continuous presence of *Clavulinoides gaultinus* (~6%), the frequent occurrence of *Spiroplectammina* sp. and *Spiroplectinata* sp. (both account for ca. 10% of the total benthic assemblage (morphogroups M2-c and M4-b, Figs. 3, 4). Dominance (D) is low throughout and never exceeds 0.4, Shannon (H) is comparatively high averaging ~2. One barren sample was recorded at 465.02 m rCCSF.

The increase in calcareous benthic foraminifera is paralleled by an increase in elemental [log]Ca/T that fluctuates between [log]Ca/T = 50 and 100 above ~467.20 m rCCSF and decreases to [log]Ca/Ti = ~50 at ~463 m rCCSF, and ultimately increase to [log]Ca/Ti = ~100 at the top of the section (Figs. 2, 4). The [log]Ba/Ti curve shows a decline from its highest values of [log]Ba/Ti = 2.8 during the low $CaCO_3$/post max-CIE transition to values slightly elevated respect to the pre-OAE 2 record that range between [log]Ba/Ti = 2.2 and 2.5 for the remainder of the section. The [log]Fe/K and [log]Fe/Zr show gradual changes above the low $CaCO_3$ interval varying from [log]Fe/K = ~1 to [log]Fe/K = ~1.5, and followed by a seemingly negative progression. Similarly, the [log]Fe/Zr ratio illustrates prominent changes at the base and through the low $CaCO_3$ interval. The [log]Fe/K curve illustrates a gradual decline from [log]Fe/K = 2 to [log]Fe/K = 1, while the [log]Fe/Zr curve shows an increase of the ratio from 1 to 2 (Fig. 2).

4.3. Hierarchical clustering and detrended correspondence analysis

Hierarchical clustering of benthic foraminifera pools the samples of the OAE 2 interval at Site U1516 in two different branches that correspond to the respective assemblages (Assemblage A and Assemblage B, see Fig. 7a, Supplementary material ST2). The position of most samples, in either Assemblage A or B, is determined by benthic foraminifera content and the results parallel the supposedly changing benthic habitats recorded in the different phases of the OAE 2. Assemblage A comprises all samples between 478.50 m rCCSF (sample U1516C-33R-4, 25–28 cm) and 470.36 m rCCSF (sample U1516C-32R-1, 43–47 cm), apart from sample U1516D-5R-1, 51–54 cm at 473.65 m rCCSF. Most samples overlying the low $CaCO_3$ interval can be found in Assemblage B (samples U1516C-31R-3, 29–31 cm at 467.27 m rCCSF through U1516C-30R-1, 50–53 cm at 459.72 m CCSF). The three samples from the low $CaCO_3$ interval plot in either branches. Samples U1516C-32R-1, 43–47 cm (470.36 m rCCSF) and U1516D-4R-3, 86–89 cm (470.28 m rCCSF) plot in Assemblage A, while sample U1516C-31R-4, 109–112 cm at 469.64 m rCCSF falls in Assemblage B. The benthic foraminiferal species characteristic of Assemblage A is *Gavelinella* sp. 3, that shows a high occurrence in every sample in this branch. This trait is shared with *Gyroidinoides* sp., instead *Globorotalites multiseptus* can only be found in four samples in Assemblage A. *Lenticulina* sp. and *Scheibnerova protindica* show higher relative abundance in Assemblage A than in Assemblage B.

Assemblage B is characterized by the high dominance of *Conorboides claytonensis* that appears in all samples, but sample U1516D-5R-1, 51–54 cm at 473.65 m rCCSF, that neither documents *Gavelinella* sp. 3 nor *Conorboides claytonensis*. Generally, Assemblage B yields higher numbers of agglutinated taxa and, in contrast to Assemblage A, *Clavulinoides gaultinus*, *Spiroplectinata* spp. and *Gaudryina pyramidata* are common elements. Another significant and abundant taxon of Assemblage B is *Praebulimina elata.* The distribution of Assemblages A and B is illustrated in Fig. 7b.

The DCA (Detrended Correspondence Analysis), calculated to explore the relationship of samples through the Cenomanian–Turonian interval, results in the alignment of samples alongside an ecologic gradient determined by foraminiferal assemblage composition. The ordination of samples and benthic foraminiferal taxa confirms the discrimination outlined in hierarchical clustering (Fig. 7c, Supplementary material ST3). The samples pre-max CIE (pre-OAE 2, low $CaCO_3$ and pre-max CIE samples) and post-max CIE samples plot almost completely separated. Interestingly, samples from the low $CaCO_3$ interval plot either together with pre-, or post-CIE samples. Samples U1516C-32R- 1, 45–48 cm (470.36 m rCCSF) and U1516D-4R-3, 86–89 cm (470.286 m rCCSF) show faunal similarities to the pre-max CIE fauna, while U1516C-31R-4, 109–112 cm (469.64 m rCCSF) can be found together with the post-max CIE group, as sample U15156D-5R-1, 51–54 cm (473.63 m rCCSF).

The differences in foraminiferal abundance along Axes 1 and 2 (Fig. 7c) represent different paleoenvironmental conditions during the Cenomanian–Turonian transition at Site U1516. Along Axis 1

b, c)) *Gyroidinoides quadratus* (showing traces of predation), U1516C-33R-4, 25–28 cm; 14a, b, c) *Globorotalites* sp., U1516D-5R-1, 127–130 cm; 15a, b, c) *Globorotalites multiseptus*, U1516D-5R-1, 127–130 cm; 16a, b, c) *Lingulogavelinella frankei*, U1516C-31R-4, 109–112 cm; 17a, b, c) *Lingulogavelinella turoniana*, U1516C-31R-4, 109–112 cm; 18,19 a, b, c) *Scheibnerova protindica*; U1516D-33R-4, 25–28 cm Scale bar = 100 μm.

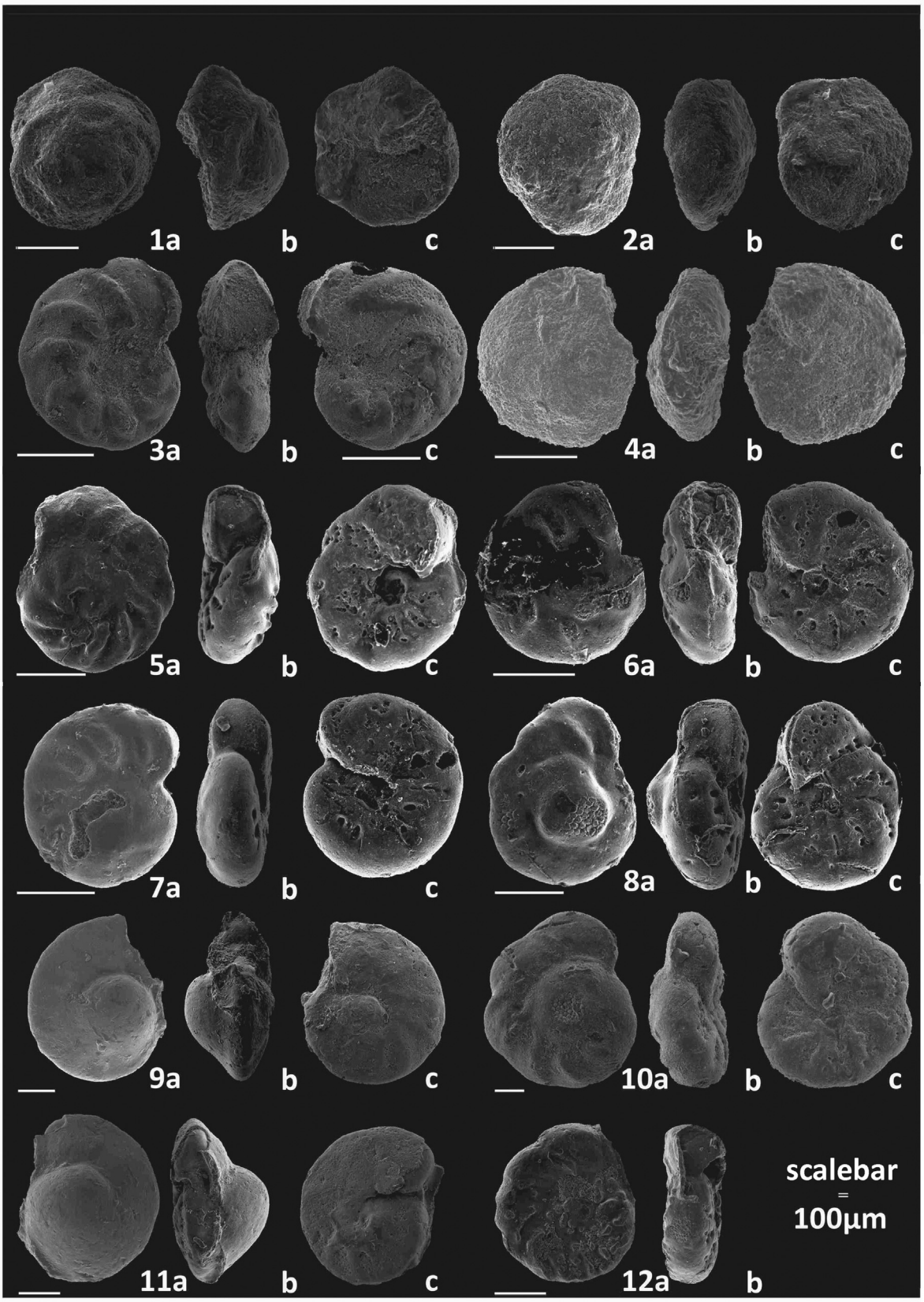

Fig. 6. SEM images of selected benthic foraminifera from Site U1516. 1) a, b, c) *Conorboides claytonensis*, U1516D-31R-4, 109–112 cm; 2 a, b, c) *Conorboides claytonensis*, U1516D-31R-4, 109–112 cm; 3 a, b, c) *Gavelinella cenomanica*, U1516D-5R-2, 125–127; 4 a, b, c) *Valvulineria* sp., U1516D-31R-4, 109–112 cm; 5 a, b, c) *Gavelinella* sp. 3, U1516C-33R-4, 25–28 cm; 6 a, b, c) *Gavelinella* sp. 3, U1516C-33R-4, 25–28 cm; 7 a, b, c*) Gavelinella* sp., U1516C-33R-4, 25–28 cm; 8 a, b, c) *Gavelinella* sp., U1516D-5R-2, 125–127 cm; 9 a, b, c) *Gavelinella intermedia*, U1516D-4r-23, 25–28 cm; 10 a, b, c) *Gavelinella vesca*, U1516C-33R-4, 25–28 cm; 11 a, b, c) *Gavelinella intermedia*, U1516D-5R-1, 127–130 cm; 12 a, b) *Stensioeina truncata*, U1516C-32R-2, 70–73 cm. Scale bar = 100 μm.

(Eigenvalue 0.59), a possible gradient in trophic levels can be inferred. Low Axis 1 − values (~0–100) are recorded in pre-OAE 2 samples and plot together with the presumably oxic taxa *Globorotalites multiseptus* (Alegret et al., 2003), and *Scheibnernova protindica*, that was interpreted as an open-ocean, upper-slope taxon in Quilty (1992). Intermediate values in Axis 1 (~100) correlate to an increase in the abundance of infaunal elongated forms (*Praebulimina, Pleurostomella* and *Dentalina*). Higher values in Axis 1 (<200), correlate to an increase in taxa that exhibited an opportunistic regime illustrated by highly abundant agglutinated (*Clavulinoides, Spiroplectinata*), *Conorboides claytonensis* and gavelinellid taxa (*Gavelinella* sp. and *Stensioeina* sp.) (Alegret et al., 2003; Friedrich et al., 2006b; Jorissen et al., 2007).

Along Axis 2 (Eigenvalue 0.32), the distance between samples could tentatively be explained by variations in the tolerance to dysoxic to suboxic environments. Fig. 7c illustrates that the differences between samples are more pronounced along Axis 1 than Axis 2. Pre- and post max-CIE samples do not show a distinct separation but a considerable overlap. A weak gradient in oxygen availability could be inferred by the high correlation of taxa tolerant of dysoxic to suboxic conditions with high values in Axis 2 (e.g., *Lenticulina, Pleurostomella* and *Gyroidinoides* and by taxa interpreted as oxic taxa, such as *Globorotalites multiseptus* (Alegret et al., 2003).

5. Discussion

5.1. Comparing the southern high latitudes biostratigraphic data to American, Atlantic and Tethyan records

The Cenomanian–Turonian benthic foraminiferal record at Site U1516 shows similarities with Site 1138 (Kerguelen Plateau, Holbourn and Kuhnt, 2002), the Cauvery Basin (Southern India, Tewari et al., 1996), and with industry wells from the north-western Australian margin (i.e., Edaggee 1, Boologooro 1 in the Southern Carnarvon basin, Haig et al., 2004). Common benthic markers recorded at Site U1516 and Site 1138 (Kerguelen Plateau) include *Praebulimina nannina*, *Pleurostomella* spp., *Tappanina laciniosa* and the agglutinated taxa *Clavulinoides gaultinus*, *Gaudryina* sp., *Bulbobaculites* sp., *Glomospira* sp. and *Spiroplectinata annectens* (Holbourn and Kuhnt, 2002). Amongst other benthic foraminiferal markers, the Cenomanian–Turonian sediments in the Cauvery Basin yield *Scheibnerova protindica* and *Gavelinella intermedia*, *Lingulogavelinella turonica, Conorboides* sp., *Praebulimina elata*. The highest occurrence of *L. turonica* was tentatively used to mark the Cenomanian–Turonian boundary (Tewari et al., 1996). Similarities between the Mentelle Basin and the Carnarvon Basin are limited to the agglutinated taxon *Bathysiphon* and to *Lenticulina* (Haig et al., 2004). Agglutinated foraminifera were thriving under low-oxygen conditions in the Cauvery Basin, but were, with reference to the taphonomic bias, rarely documented at Site 1138 (Holbourn and Kuhnt, 2002; Tewari et al., 1996). The benthic foraminiferal datasets from the Kerguelen Plateau and the Cauvery Basin show barren intervals or impoverished assemblages and black shales during the latest Cenomanian − earliest Turonian and within the *Whiteinella archaeocretacea* planktonic foraminifera Zone (Holbourn and Kuhnt, 2002). Comparable to Site U1516, Site 1138 and the Cauvery Basin record show a repopulation in benthic foraminifera after the OAE 2. Specifically, the assemblage at the Kerguelen Plateau documents changes in the abundance of taxa that might be related to environmental change rather than to extinctions.

Biostratigraphic similarities of the Mentelle Basin record with the Cenomanian–Turonian benthic foraminiferal assemblages of the epeiric Western Interior Seaway (WIS) in the Rock Canyon section can be found at the genus level. During the OAE 2, most localities in the WIS record rare agglutinated taxa and document the reduced abundance of benthic foraminifera (Eicher and Worstell, 1970; Leckie et al., 1998; Elderbak et al., 2014; Lowery et al., 2014; Elderbak and Leckie, 2016; Lowery and Leckie, 2017). Apart from generally low benthic foraminiferal diversity through the Cenomanian-Turonian transition, selected levels rich in calcareous benthic foraminifera (the upper Cenomanian "Benthonic Zone" of Eicher and Worstell, 1970) yield therein plentiful gavelinellids (*Lingulogavelinella, Gavelinella*) and other trochospiral benthic taxa. A similar pattern in benthic foraminiferal recovery was observed after the main CIE at Site U1516.

The tropical Atlantic record from Demerara Rise (ODP Leg 207, Friedrich and Erbacher, 2006) demonstrates more biostratigraphic affinities at species level to the high southern latitudes assemblages than to the WIS record. Friedrich et al. (2006a) and Friedrich and Erbacher (2006) documented the occurrence of *Praebulimina elata, Gavelinella cenomanica* and other cosmopolitan benthic foraminifera that are also recorded at Site U1516. However, at Site U1516 we did not record *Neubulimina albertensis,* which was frequently documented at Demerara Rise and in the WIS.

The OAE 2 in the northwest European record of Eastbourne (UK) presents a cosmopolitan deep water assemblage (Paul et al., 1999) composed by agglutinated *Spiroplectammina, Tritaxia,* cosmopolitan calcareous taxa like *Gavelinella cenomanica* and other osangularids and gavelinellids (*Osangularia* sp. A, *G. baltica, G. reussi, G. berthelini*).

The greater part of Central Tethyan localities in Romania, Russia and Ukraine are mostly barren of benthic foraminifera at the Cenomanian–Turonian transition. Starting with the upper Cenomanian *Rotalipora cushmani* Zone, the dominance of radiolaria and the virtual absence of benthic foraminifera depicts deteriorated paleoenvironmental conditions in the Carpathian sections (Cetean et al., 2008). Biostratigraphic similarities to the austral record are supported by the rare occurrence of *Gavelinella vesca* and *Gavelinella cenomanica* that have been documented from the Tethyan settings in Central, Eastern and Western Europe and Asia (e.g. *G. vesca* from Dubivtsi, Western Ukraine, Dubicka and Peryt, 2012 and *G. cenomanica* from Eastbourne, Paul et al., 1999; southern Tajikistan, Korchagin, 2004; Betic Cordillera, Spain, Reolid et al., 2016; Lower Saxony, Niebuhr et al., 1999; Briansk, Walaszczyk et al., 2004).

Foraminiferal data from a slope setting characterized by high detrital influx in the eastern Tethyan Kopet Dagh Basin in Iran (Kalanat et al., 2017) are similar to assemblages observed in the Mentelle Basin. They are composed by abundant praebuliminids, lenticulinids, gavelinellids (and other trochospiral taxa like *Lingulogavelinella* or *Valvulineria*) and agglutinated cosmopolitan taxa including *Lagenammina, Ammosphaeroidina, Tritaxia* and *Reophax.* Moreover, the Iranian record in the upper Cenomanian (lower to middle *W. archaeocretacea* Zone) sediments illustrates an interval barren of foraminifera followed by common agglutinated taxa, whereas in lower Turonian sediments calcareous taxa dominate the interval after the OAE 2.

A common feature exemplified by comparable records of the OAE 2 interval is the stepwise reduction in the total abundance of benthic foraminifera. During the lower third of the OAE 2 interval, that correlates to the uppermost Cenomanian Plenus Marls at Eastbourne, repopulation events register higher numbers of benthic foraminifera that might correspond to the Plenus Cold Event or the WIS Benthonic Zone (Petrizzo et al., 2021a). Petrizzo et al. (2021a) correlated the $\delta^{13}C$ curve of Site U1516 to the carbon isotope record at Eastbourne (UK) and questionably identified the Plenus Cold Event (Jenkyns et al., 2017; O'Connor et al., 2020) at approximately 473.02 m rCCSF. However, neither significant changes in benthic nor

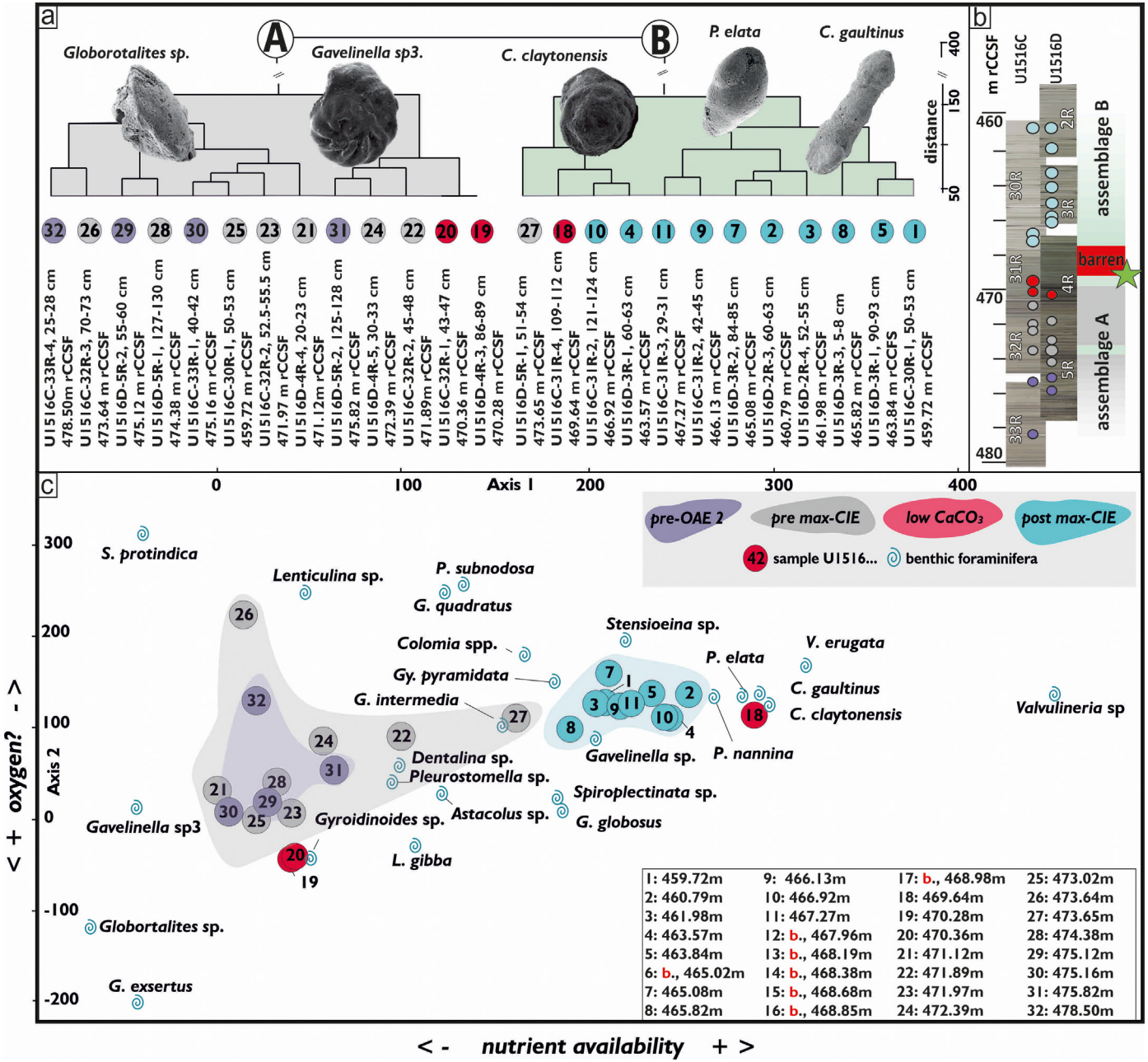

Fig. 7. a) Hierarchical clustering (after Ward, 1963) of samples encompassing the OAE 2 interval at IODP Site U1516. Samples cluster in two branches: A (grey) with determinant benthic foraminiferal taxa *Globorotalites* sp. and *Gavelinella* sp. 3, and B (green), with determinant taxa *Conorboides claytonensis*, *Praebulimina elata* and the agglutinated foraminifera *Clavulinoides gaultinus*. Due to limited space, datapoints representing different samples are colour coded according to their location (see Figs. 3, 4) and assigned next to their number designation. b) distribution of dominant assemblage types through Holes U1516C and U1516D according to hierarchical clustering. The star marks the max-CIE level at 469.04 m rCCSF. c) Detrended Correspondence Analysis of colour-coded samples of pre-OAE 2, pre-max CIE, low $CaCO_3$ and post-max CIE intervals and benthic foraminiferal abundance data. Circles represent samples, blue spirals represent benthic foraminiferal taxa. Based on environmental preferences of benthic taxa, Axis 1 and Axis 2 represent environmental interpretations (different trophic and oxygen levels, respectively). Legend in the top right elaborates the colour coding and the position of samples. b = barren.

planktonic foraminiferal assemblages were observed at Site U1516 (Figs. 3, 4).

5.2. A stressed benthic foraminifera fauna

Below 470 m rCCSF, the benthic foraminiferal community documents relatively few exclusively infaunal taxa (14% of the benthic assemblage below 470 m rCCSF, compared to 30% above the max-CIE interval, Fig. 8). After the pre OAE 2 Interval, the bottom waters were increasingly influenced by eutrophication (and high fluctuations in primary-/export productivity reflected in the [log] Ba/Ti signature, particularly between 472 and 470 m rCCSF) and elevated freshwater runoff that promoted changes in associated density gradients and a reduced bottom water ventilation (Chen et al., 2022). Consequently, the pre max-CIE interval must have experienced an increase in hypoxia that did affect the epifaunal benthic habitats and reached below the sediment water interface layers. Apart from the lack of dissolved oxygen in the infaunal habitats, the comparatively rare occurrence of infaunal taxa could furthermore be explained by taphonomic processes and/or dissolution of test material. For instance, agglutinated taxa can suffer from dissolution and degradation of organic cement and have limited preservation potential during early diagenesis. Therefore, resilient calcareous epifaunal taxa in a depauperate, stressed assemblage are recorded in this interval (Kaminski et al., 1995; Kuhnt et al., 1996; Sierro et al., 2003; Murray and Alve, 2011). Benthic foraminiferal abundance was already in a declining phase during the upper part of the pre max-CIE interval, corresponding to a significant drop in Ca (see Figs. 2, 4, 8). The overlying low-$CaCO_3$ interval correlates with steady low Ca values and coincides with elevated silica production as reflected by the abundance of radiolaria (Petrizzo et al., 2022, 2021a; Chen et al., 2022). According to the latter observations and to ongoing eutrophication and radically limited oxygen supply, benthic foraminifera must have found an increasingly hostile environment for test sequestration and reproduction (between ~474 m rCCSF to 469.46 m rCCSF, Fig. 8).

A different picture of the benthic foraminiferal assemblage is presented in sample U1516C-31R-4, 109–112 cm (469.46 m rCCSF) (see Fig. 8). This sample tentatively correlates to a short interval prior to a drastic increase in bioproductivity exemplified by a positive excursion of the [log]Ba/Ti signature ranging from [log]Ba/Ti = ~1.5 to [log]Ba/Ti = ~1.8 between 470 m rCCSF and 468.7 m rCCSF and by the peak CIE excursion at 469.04 m rCCSF (Petrizzo et al., 2021a, 2022). Directly underlying this interval (at 470.6 m rCCSF), a seemingly insignificant excursion in [log]Ca/Ti from [log] Ca/Ti = ~1.1 to 11.8 is documented. Effects of a slight increase in the [log]Ca/Ti signature were possibly dampened by an undersaturation in Ca (and oversaturation in Si, promoting dissolution of calcite), linked to the overly high abundance of radiolaria as well as elevated freshwater runoff, and associated changes in the stratification of the water masses (Petrizzo et al., 2021a, 2022; Chen et al., 2023, 2022).

The reason for elevated alkalinity levels and reduced bottom water acidification that facilitated the preservation of a presumably autochthonous, well preserved, and comparatively diversified benthic foraminiferal assemblage at 469.64 m rCCSF remains unidentified and a matter of speculation (similar settings are documented in e.g., Friedrich et al., 2010; Jenkyns, 2010; Ohkouchi et al., 2015). Despite ongoing eutrophication, low alkalinity levels and presumable hypoxia, this sample yields a benthic foraminiferal assemblage with abundant calcareous and agglutinated foraminifera (see Figs. 3, 4, 8). It seems reasonable to assume an unstable pattern in terrigenous supply and runoff during the reorganisation of catchment areas as well as changes in nutrient provenance as illustrated by variations in clay mineralogy and major changes in the ratios of Fe/K and Fe/Zr, that could have been associated to the increased ventilation of bottom waters (see Fig. 2, Chen et al., 2022, 2023). The increasing export productivity and the associated oversupply of nutrients might, for a brief period, have made up for the undersaturation in oxygen and could have benefitted both the foraminiferal and the radiolarian assemblages (i.e., Holbourn and Kuhnt, 2002; Friedrich et al., 2006a; Murray and Alve, 2011).

5.3. Timing of the benthic foraminiferal assemblage changes

The two distinctly different benthic foraminiferal assemblages (see Figs. 7b and 8) illustrate a distribution that mostly correlates to the different phases of the OAE 2 identified in Petrizzo et al. (2021a). Assemblage A was identified exclusively below the barren intervals recorded during the low $CaCO_3$ interval and the max CIE. Assemblage B can be identified in samples U1516D-5R-1, 51–54 cm (473.65 m rCCSF) and U1516C-31R-4, 109–112 cm (469.46 m rCCSF) located in the pre-max CIE and low $CaCO_3$ interval, respectively (see section 4.3 and Figs. 7a, b). The similarity of Sample U1516D-5R-1, 51–54 cm (473.65 m rCCSF) to other samples falling in Assemblage A can be explained by the absence of the indicative marker taxa of Assemblage A and B (*Gavelinella* sp. 3 and *Conorboides claytonensis*, respectively).

Sample U1516C-31R-4109–112 cm at 469.46 m rCCSF (Fig. 3) is markedly different as it shows an assemblage that differs from the previous and, apart from an increase in *Gavelinella* and *Conorboides,* yields taxa resembling the pre-OAE 2 interval rather than the pre max-CIE interval or the remainder part of the low $CaCO_3$ interval. Remarkably, benthic foraminiferal assemblage changes do not seem triggered by perturbation during the main phase of the OAE 2 and the CIE (Fig. 8), but are rather registered during the low $CaCO_3$ interval, presumably characterized by high productivity with sporadically associated black shale deposition (Petrizzo et al., 2021a; Chen et al., 2022). Environmental changes registered in bottom waters are merely interrupted by the max-CIE.

5.4. Reclaiming infaunal habitats

The infaunal agglutinated taxa (*Clavulinoides gaultinus*, *Spiroplectammina*) and infaunal calcareous taxa (*Praebulimina*), that were absent during the pre max-CIE and most of the low $CaCO_3$ interval, are returning above the max CIE. Compared to the pre-CIE assemblages that are predominantly represented by Assemblage A in hierarchical clustering (Fig. 7), the post max-CIE assemblage (mostly Assemblage B) is equally indicative for dysoxic environments and yields a number of marker taxa for high organic matter flux and eutrophic environments such as the infaunal opportunistic calcareous taxa *Praebulimina* (*P. elata, P. nanina*) and *Pleurostomella*, the infaunal opportunistic agglutinated taxa (*Clavulinoides gaultinus, Gaudryina pyramidata, Spiroplectinata, Spiroplectammina*), and the epifaunal gavelinellids and osangularids (Coccioni and Galeotti, 2003; Holbourn and Kuhnt, 2002; Koutsoukos et al., 1990; Koutsoukos and Hart, 1990; Widmark and Speijer, 1997; see Section 4, Figs. 3, 4).

A variety of paleoenvironmental factors could play a role in the repopulation of infaunal habitats and the shift from dominant Assemblage A to Assemblage B (Figs. 7a, 7b, 8). A global sea level highstand is proposed during the Cenomanian–Turonian transition (Haq et al., 1987; Haq, 2014; Miller et al., 2005). A sustained rise in sea level continuing through the low $CaCO_3$ and post max-CIE intervals, together with changes in terrigenous runoff and bottom water ventilation patterns, could have caused the progression from an outer shelf to an upper slope environment. Specifically, the benthic foraminiferal assemblages in the post max-CIE interval might have benefitted from ongoing riverine influx at Site U1516. The upward decreasing $\delta^{13}C$ values coincide with benthic

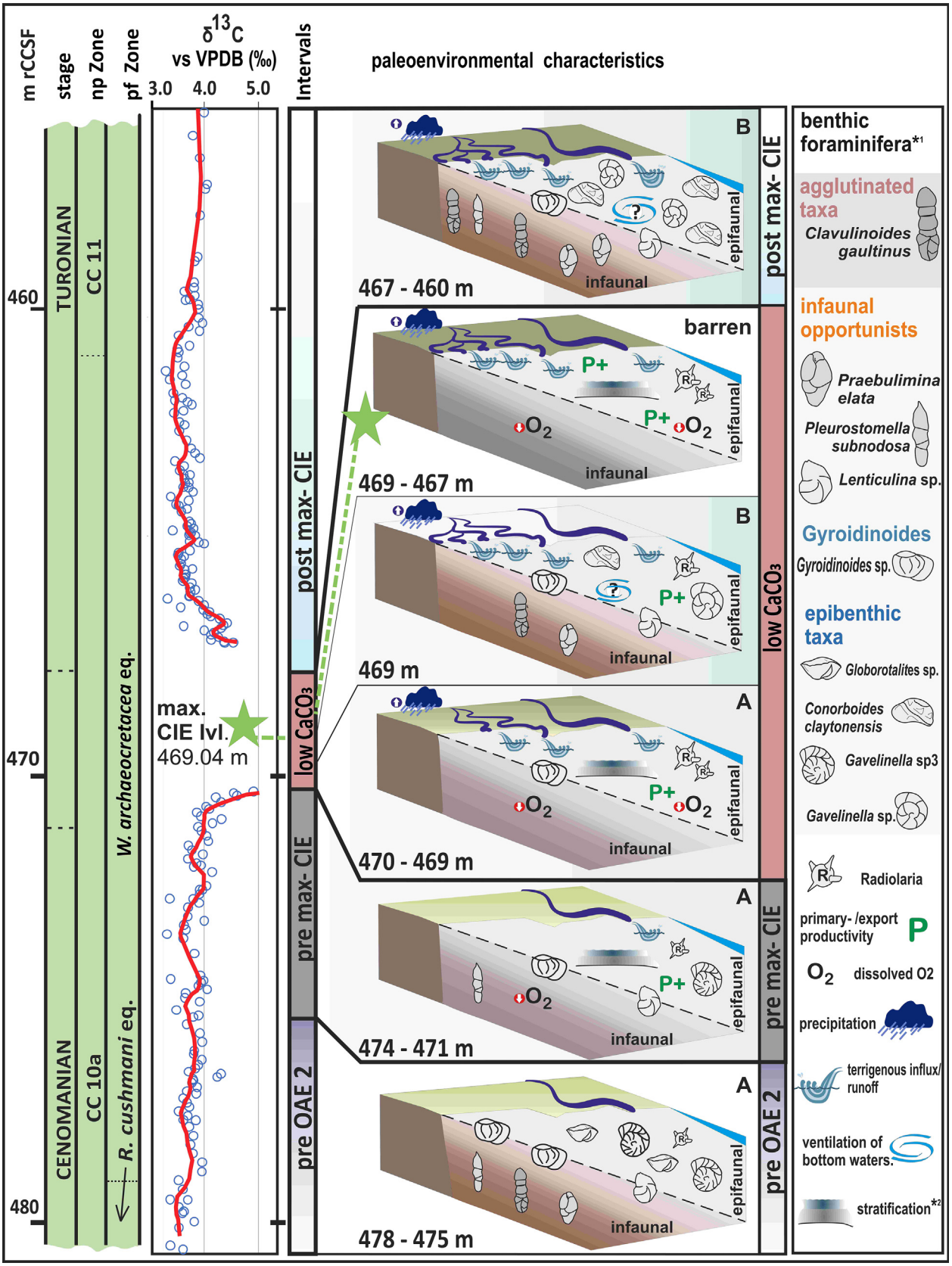

Fig. 8. Biostratigraphic framework, $\delta^{13}C$ curve and Intervals according to Petrizzo et al. (2021a, 2022) and this study. Palaeoecological features of the environmental intervals are based on foraminiferal assemblage data indicating branch A and B, respectively (see Fig. 7), see legend on the right-hand side of the figure. (*1) Pictograms of benthic foraminifera to indicate the most common benthic foraminiferal taxa; (*2) increased stratification of bottom and surface waters.

foraminiferal assemblages that repopulated the bottom waters and presumably benefitted from an excess supply of nutrients. A complete reorganization of runoff patterns as outlined in Chen et al. (2022), could have increased the ventilation of bottom waters and fostered the (re)colonization of infaunal habitats by taxa tolerant of dysoxic to suboxic environments (Van Wagoner et al., 1988; Leckie and Olson, 2003).

5.5. Opportunist epibenthic foraminifera

The post max-CIE interval records distinct changes in respect to dominant taxa: the taxon *Gavelinella* sp. 3, a dominant element in Assemblage A, is almost completely replaced in favour of other biconvex, low trochospiral gavelinellids, *Stensioeina* spp. and *Conorboides claytonensis* occurring in Assemblage B (Fig. 7a). The high increase of foraminiferal abundance, together with profoundly increasing Ca values and slightly elevated Ba values, suggests a higher availability of food in a marked eutrophic regime.

Gavelinellids, that were reported as opportunistic taxa in the sense of Kauffman and Harries (1966) in the Cretaceous (Schmiedl et al., 1997; Holbourn and Moullade, 1998; Holbourn, 2001; Holbourn and Kuhnt, 2002; Alegret et al., 2003; Murray, 2006; Friedrich et al., 2006b; Alegret, 2007; Elderbak and Leckie, 2016), and the high trochospire morphotype *Conorboides* could have tolerated low oxygen conditions if there is high food availability. However, Herrle et al. (2003) interpreted *Gavelinella* as eutrophic indicator that is absent under poor oxygenation in the Aptian-Albian record of the Vocontian basin. *Gavelinella*'s species are often described as epifaunal pioneer species that take advantage of increasing food supply and lack of competition (see Holbourn and Kuhnt, 2002; Friedrich, 2010). The increase in opportunist epibenthic taxa, such as *Gavelinella* and *Conorboides* is an indicator that changes in microfossil assemblages, in particular changes from Assemblage A to Assemblage B during the OAE 2 interval at Site U1516, were impacted by food supply rather than the increased availability of oxygen.

6. Conclusions

1. International Ocean Discovery Program (IODP) Expedition 369 Australia Cretaceous Climate and Tectonics recovered a record of the Oceanic Anoxic Event 2 (OAE 2) in the Mentelle Basin at Site U1516 in a proximal, outer neritic to upper bathyal setting. This paper documents the composition and changes of the benthic foraminiferal assemblage through the Cenomanian–Turonian transition and the OAE 2.
2. Four significantly different intervals named the pre OAE, pre max-CIE (Carbonate Isotope Excursion), low $CaCO_3$, and post low $CaCO_3$ interval were identified according to variations in benthic foraminiferal assemblages. Through these intervals we document a decline in density and taxonomic richness of the benthic foraminiferal assemblage, a paleoenvironmental setting barren of benthic foraminifera during the main phase of OAE 2, and a repopulation event after the increased carbon burial that follows the main phase of the OAE 2.
3. Cosmopolitan benthic foraminiferal taxa recorded at Site U1516 can be correlated globally to other localities revealing similar paleoenvironmental conditions at bottom waters across the Cenomanian–Turonian transition.
4. At Site U1516, two different types of benthic foraminiferal assemblages have been identified. Assemblage A illustrates a depauperate community with significantly lower numbers of benthic foraminifera per gram of dry sediment. On the contrary, Assemblage B yields a higher taxonomic diversity as well as a higher number of individuals. Both Assemblages A and B reflect low oxygen tolerant communities that were probably controlled by nutrient availability. The timing of the foraminiferal assemblage change suggests that environmental changes registered in the bottom waters are merely interrupted by the Carbon Isotope Excursion.
5. The paleoenvironmental changes illustrated by the benthic foraminiferal assemblage at Site U1516 were mostly influenced by food supply rather than fluctuations in the oxygen availability.

Acknowledgements

The Authors are indebted to the editor Eduardo Koutsoukos, and to Ellen Thomas and an anonymous reviewer for their comments and suggestions that greatly improved the quality of the manuscript. EW thanks the Austrian Science Fund (FWF) grant Nr. J-4444B and the International Ocean Discovery Program (IODP) for samples. MRP acknowledges financial support by IODP-Italia and CNR-Italian National Research Council (projects CONTR_CNR17MPETR_01 and CONTR_CNR19MPETR_01) to perform activities related to European Consortium for Ocean Research Drilling and IODP, and the support of the Italian Ministry of University and Research (MUR) projects PRIN 2017RX9XXY (E. Erba scientific coordinator).

References

Alegret, L., 2007. Recovery of the deep-sea floor after the Cretaceous–Paleogene boundary event: the benthic foraminiferal record in the Basque–Cantabrian basin and in South-eastern Spain. Palaeogeography, Palaeoclimatology, Palaeoecology 1–2, 181–194. https://doi.org/10.1016/j.palaeo.2007.02.047.

Alegret, L., Molina, E., Thomas, E., 2003. Benthic foraminiferal turnover across the Cretaceous/Paleogene boundary at Agost (southeastern Spain): paleoenvironmental inferences. Marine Micropaleontology 48, 251–279. https://doi.org/10.1016/S0377-8398(03)00022-7.

Alegret, L., Ortiz, S., Molina, E., 2009. Extinction and recovery of benthic foraminifera across the Paleocene–Eocene thermal maximum at the Alamedilla section (Southern Spain). Palaeogeography, Palaeoclimatology, Palaeoecology 279, 186–200. https://doi.org/10.1016/j.palaeo.2009.05.009.

Bąk, K., Bąk, M., Geroch, S., Manecki, M., 1997. Biostratigraphy and paleoenvironmental analysis of benthic Foraminifera and radiolarians in Paleogene variegated shales in the Skole Unit, Polish Flysch Carpathians. Annales Societatis Geologorum Poloniae 67, 135–154.

Barclay, R.S., McElwain, J.C., Sageman, B.B., 2010. Carbon sequestration activated by a volcanic CO_2 pulse during Ocean Anoxic Event 2. Nature Geoscience 3, 205–208. https://doi.org/10.1038/ngeo757.

Bernhard, J.M., 1986. Characteristic assemblages and Morphologies of benthic foraminifera from anoxic, organic-rich deposits: Jurassic through Holocene. Journal of Foraminiferal Research 16, 207–215.

Bertrand, S., Hughen, K., Giosan, L., 2015. Limited influence of sediment grain size on elemental XRF core scanner measurements. In: Croudace, I.W., Rothwell, R.G. (Eds.), Micro-XRF Studies of Sediment Cores, Developments in Paleoenvironmental Research. Springer Netherlands, Dordrecht, pp. 473–490. https://doi.org/10.1007/978-94-017-9849-5_19.

Bogus, K., Batenburg, S., Jones, M., Edgar, Kirsty, De Vleeschouwer, D., Tagliaro, G., Martinez, M., Hanson, E., Walker-Trivett, C., Levay, B., Schoemann, M., 2019. Shore-based X-ray fluorescence core scanning of IODP expedition 369 (Australia Cretaceous Climate and Tectonics) material. In: Proc. Int. Ocean Discov. Program 369 Suppl. Mater., vol. 369. Integrated Ocean Drilling Program Management International, Inc.

Bomou, B., Adatte, T., Tantawy, A.A., Mort, H., Fleitmann, D., Huang, Y., Föllmi, K.B., 2013. The expression of the Cenomanian–Turonian oceanic anoxic event in Tibet. Palaeogeography, Palaeoclimatology, Palaeoecology 369, 466–481. https://doi.org/10.1016/j.palaeo.2012.11.011.

Bowman, A.R., Bralower, T.J., 2005. Paleoceanographic significance of high-resolution carbon isotope records across the Cenomanian–Turonian boundary in the Western Interior and New Jersey coastal plain, USA. Marine Geology 217, 305–321. https://doi.org/10.1016/j.margeo.2005.02.010.

Caron, M., Dall'Agnolo, S., Accarie, H., Barrera, E., Kauffman, E.G., Amédro, F., Robaszynski, F., 2006. High-resolution stratigraphy of the Cenomanian–Turonian boundary interval at Pueblo (USA) and wadi Bahloul (Tunisia): stable isotope and bio-events correlation. Geobios 39, 171–200. https://doi.org/10.1016/j.geobios.2004.11.004.

Carter, S.C., PAytan, A., Griffith, E.M., 2020. Toward an improved understanding of the marine barium cycle and the application of marine barite

as a paleoproductivity proxy. Minerals 10, 421. https://doi.org/10.3390/min10050421.
Cetean, C.G., Balc, R., Kaminski, M.A., Filipescu, S., 2008. Biostratigraphy of the Cenomanian-Turonian boundary in the Eastern Carpathians (Dâmbovița Valley): preliminary observations. Studia Universitatis Babes-Bolyai: Geologia 53 (1), 11–23.
Cetean, C.G., Balc, R., Kaminski, M.A., Filipescu, S., 2011. Integrated biostratigraphy and palaeoenvironments of an upper Santonian – upper Campanian succession from the southern part of the Eastern Carpathians, Romania. Cretaceous Research 32 (5), 575–590.
Chen, H., Xu, Z., Bayon, G., Lim, D., Batenburg, S.J., Petrizzo, M.R., Hasegawa, T., Li, T., 2022. Enhanced hydrological cycle during Oceanic Anoxic Event 2 at southern high latitudes: new insights from IODP Site U1516. Global and Planetary Change 209, 103735. https://doi.org/10.1016/j.gloplacha.2022.103735.
Chen, H., Bayon, G., Xu, Z., Li, T., 2023. Hafnium isotope evidence for enhanced weatherability at high southern latitudes during Oceanic Anoxic Event 2. Earth and Planetary Science Letters 601, 117910. https://doi.org/10.1016/j.epsl.2022.117910.
Coccioni, R., Galeotti, S., 2003. The middle-Cenomanian Event: prelude to OAE 2. Palaeogeography, Palaeoclimatology, Palaeoecology 190, 427–440. https://doi.org/10.1016/S0031-0182(02)00617-X.
Corentin, P., Deconinck, J.-F., Pellenard, P., Amédro, F., Bruneau, L., Chenot, E., Matrion, B., Huret, E., Landrein, P., 2020. Environmental and climatic controls of the clay mineralogy of Albian deposits in the Paris and Vocontian basins (France). Cretaceous Research 108, 104342.
Corliss, B.H., 1985. Microhabitats of benthic foraminifera within deep-sea sediments. Nature 314, 435–438.
Corliss, B.H., Chen, C., 1988. Morphotype patterns of Norwe- gian Sea deep-sea benthic foraminifera and ecological implications. Geology 16, 716–719.
Croudace, I.W., Rothwell, R.G. (Eds.), 2015. Micro-XRF Studies of Sediment Cores: Applications of a Non-destructive Tool for the Environmental Sciences, Developments in Paleoenvironmental Research. Springer Netherlands, Dordrecht. https://doi.org/10.1007/978-94-017-9849-5.
Desmares, D., Crognier, N., Bardin, J., Testé, M., Beaudoin, B., Grosheny, D., 2016. A new proxy for Cretaceous paleoceanographic and paleoclimatic reconstructions: coiling direction changes in the planktonic foraminifera Muricohedbergella delrioensis. Palaeogeography, Palaeoclimatology, Palaeoecology 445, 8–17. https://doi.org/10.1016/j.palaeo.2015.12.021.
Dickens, G.R., Fewless, T., Thomas, E., Bralower, T.J., 2003. Excess barite accumulation during the Paleocene-Eocene thermal maximum: massive input of dissolved barium from seafloor gas hydrate reservoirs. In: Wing, S.L., Gingerich, P.D., Schmitz, B., Thomas, E. (Eds.), Causes and Consequences of Globally Warm Climates in the Early Paleogene: Boulder, Colorado, Geological Society of America Special Paper 369, 11–23.
Dickson, A.J., Saker-Clark, M., Jenkyns, H.C., Bottini, C., Erba, E., Russo, F., Gorbanenko, O., Naafs, B.D.A., Pancost, R.D., Robinson, S.A., van den Boorn, S.H.J.M., Idiz, E., 2017. A Southern Hemisphere record of global trace-metal drawdown and orbital modulation of organic-matter burial across the Cenomanian–Turonian boundary (Ocean Drilling Program Site 1138, Kerguelen Plateau). Sedimentology 64, 186–203. https://doi.org/10.1111/sed.12303.
Direen, N.G., Stagg, H.M.J., Symonds, P.A., Colwell, J.B., 2008. Architecture of volcanic rifted margins: new insights from the Exmouth – Gascoyne margin, Western Australia. Australian Journal of Earth Sciences 55, 341–363. https://doi.org/10.1080/08120090701769472.
Du Vivier, A.D.C., Selby, D., Sageman, B.B., Jarvis, I., Gröcke, D.R., Voigt, S., 2014a. Marine 187Os/188Os isotope stratigraphy reveals the interaction of volcanism and ocean circulation during Oceanic Anoxic Event 2. Earth and Planetary Science Letters 389, 23–33. https://doi.org/10.1016/j.epsl.2013.12.024.
Dubicka, Z., Peryt, D., 2012. Foraminifers and stable isotope record of the Dubivtsi chalk (upper Turonian, Western Ukraine): palaeoenvironmental implications. Geological Quarterly 199–214.
Eicher, D.L., Worstell, P., 1970. Cenomanian and Turonian Foraminifera from the Great Plains, United States. Micropaleontology 16, 269. https://doi.org/10.2307/1485079.
Elderbak, K., Leckie, R.M., 2016. Paleocirculation and foraminiferal assemblages of the Cenomanian–Turonian Bridge Creek Limestone bedding couplets: productivity vs. dilution during OAE2. Cretaceous Research 60, 52–77. https://doi.org/10.1016/j.cretres.2015.11.009.
Elderbak, K., Leckie, R.M., Tibert, N.E., 2014. Paleoenvironmental and paleoceanographic changes across the Cenomanian–Turonian Boundary Event (Oceanic Anoxic Event 2) as indicated by foraminiferal assemblages from the eastern margin of the Cretaceous Western Interior Sea. Palaeogeography, Palaeoclimatology, Palaeoecology 413, 29–48. https://doi.org/10.1016/j.palaeo.2014.07.002.
Eldrett, J.S., Minisini, D., Bergman, S.C., 2014. Decoupling of the carbon cycle during Ocean Anoxic Event 2. Geology 42, 567–570. https://doi.org/10.1130/G35520.1.
Erba, E., 2004. Calcareous nannofossils and Mesozoic oceanic anoxic events. Marine Micropaleontology 52, 85–106. https://doi.org/10.1016/j.marmicro.2004.04.007.
Erbacher, J., Friedrich, O., Wilson, P.A., Birch, H., Mutterlose, J., 2005. Stable organic carbon isotope stratigraphy across Oceanic Anoxic Event 2 of Demerara Rise, western tropical Atlantic: carbon isotope stratigraphy. Geochemistry, Geophysics, Geosystems 6. https://doi.org/10.1029/2004GC000850.
Forster, A., Schouten, S., Moriya, K., Wilson, P.A., Sinninghe Damsté, J.S., 2007. Tropical warming and intermittent cooling during the Cenomanian/Turonian oceanic anoxic event 2: sea surface temperature records from the equatorial Atlantic: tropical cenomanian/turonian SST records. Paleoceanography 22, 1. https://doi.org/10.1029/2006PA001349.
Forster, A., Kuypers, M.M.M., Turgeon, S.C., Brumsack, H.-J., Petrizzo, M.R., Sinninghe Damsté, J.S., 2008. The Cenomanian/Turonian oceanic anoxic event in the South Atlantic: New insights from a geochemical study of DSDP Site 530A. Palaeogeography, Palaeoclimatology, Palaeoecology 267, 256–283. https://doi.org/10.1016/j.palaeo.2008.07.006.
Frenzel, P., 2000. Die benthischen Foraminiferen der Rügener Schreibkreide (Unter-Maastrichtium, NE-Deutschland). Neue Palaontologische Abhandlungen 3, 361pp (Dresden).
Friedrich, O., 2010. Benthic foraminifera and their role to decipher paleoenvironment during middle-Cretaceous Oceanic Anoxic Events – the "anoxic benthic foraminifera" paradox. Revue de Micropaléontologie 53, 175–192. https://doi.org/10.1016/j.revmic.2009.06.001.
Friedrich, O., Erbacher, J., 2006. Benthic foraminiferal assemblages from Demerara Rise (ODP Leg 207, western tropical Atlantic): possible evidence for a progressive opening of the Equatorial Atlantic Gateway. Cretaceous Research 27, 377–397. https://doi.org/10.1016/j.cretres.2005.07.006.
Friedrich, O., Hemleben, C., 2007. Early Maastrichtian benthic foraminiferal assemblages from the western North Atlantic (Blake Nose) and their relation to paleoenvironmental changes. Marine Micropaleontology 62, 31–44.
Friedrich, O., Erbacher, J., Mutterlose, J., 2006a. Paleoenvironmental changes across the Cenomanian/Turonian Boundary Event (Oceanic Anoxic Event 2) as indicated by benthic foraminifera from the Demerara Rise (ODP Leg 207). Revue de Micropaléontologie 49, 121–139. https://doi.org/10.1016/j.revmic.2006.04.003.
Friedrich, O., Schmiedl, G., Erlenkeuser, H., 2006b. Stable isotope composition of Late Cretaceous benthic foraminifera from the southern South Atlantic: biological and environmental effects. Marine Micropaleontology 58, 135–157. https://doi.org/10.1016/j.marmicro.2005.10.005.
Friedrich, O., Norris, R.D., Erbacher, J., 2012. Evolution of middle to Late Cretaceous oceans—A 55 m.y. record of Earth's temperature and carbon cycle. Geology 40, 107–110. https://doi.org/10.1130/G32701.1.
Gaina, C., Müller, R.D., Brown, B., Ishihara, T., Ivanov, S., 2007. Breakup and early seafloor spreading between India and Antarctica. Geophysical Journal International 170, 151–169. https://doi.org/10.1111/j.1365-246X.2007.03450.x.
Gale, A.S., Jenkyns, H.C., Tsikos, H., van Breugel, Y., Sinninghe Damsté, J.S., Bottini, C., Erba, E., Russo, F., Falzoni, F., Petrizzo, M.R., Dickson, A.J., Wray, D.S., 2019. High-resolution bio- and chemostratigraphy of an expanded record of Oceanic Anoxic Event 2 (Late Cenomanian–Early Turonian) at Clot Chevalier, near Barrème, SE France (Vocontian Basin). Newsletters on Stratigraphy 52, 97–129. https://doi.org/10.1127/nos/2018/0445.
Gangl, S.K., Moy, C.M., Stirling, C.H., Jenkyns, H.C., Crampton, J.S., Clarkson, M.O., Ohneiser, C., Porcelli, D., 2019. High-resolution records of Oceanic Anoxic Event 2: insights into the timing, duration and extent of environmental perturbations from the palaeo-South Pacific Ocean. Earth and Planetary Science Letters 518, 172–182. https://doi.org/10.1016/j.epsl.2019.04.028.
Gebhardt, H., 2006. Resolving the calibration problem in Cretaceous benthic foraminifera paleoecological interpretation: Cenomanian to Coniacian assemblages from the Benue Trough analyzed by conventional methods and correspondence analysis. Micropaleontology 52, 151–176. https://doi.org/10.2113/gsmicropal.52.2.151.
Gebhardt, H., Sarnthein, M., Grootes, P.M., Kiefer, T., Kuehn, H., Schmieder, F., Röhl, U., 2008. Paleonutrient and productivity records from the subarctic North Pacific for Pleistocene glacial terminations I to V: paleoproductivity north pacific. Paleoceanography 23. https://doi.org/10.1029/2007PA001513.
Gertsch, B., Keller, G., Adatte, T., Berner, Z., Kassab, A.S., Tantawy, A.A.A., El-Sabbagh, A.M., Stueben, D., 2010. Cenomanian–Turonian transition in a shallow water sequence of the Sinai, Egypt. International Journal of Earth Sciences 99, 165–182. https://doi.org/10.1007/s00531-008-0374-4.
Gibbons, A.D., Barckhausen, U., van den Bogaard, P., Hoernle, K., Werner, R., Whittaker, J.M., Müller, R.D., 2012. Constraining the Jurassic extent of Greater India: tectonic evolution of the West Australian margin. Geochemistry, Geophysics, Geosystems 13, Q05W13. https://doi.org/10.1029/2011GC003919.
Govin, A., Holzwarth, U., Heslop, D., Ford Keeling, L., Zabel, M., Mulitza, S., Collins, J.A., Chiessi, C.M., 2012. Distribution of major elements in Atlantic surface sediments (36°N-49°S): imprint of terrigenous input and continental weathering. Geochemistry, Geophysics, Geosystems 13, Q01013. https://doi.org/10.1029/2011GC003785.
Govindan, A., Ramesh, P., 1995. Cretaceous anoxic events and their role in generation and accumulation of hydrocarbon in Cauvery Basin, India. Indian Journal of Petroleum Geology 4, 1–15.
Grosheny, D., Ferry, S., Lécuyer, C., Thomas, A., Desmares, D., 2017. The Cenomanian–Turonian Boundary Event (CTBE) on the southern slope of the Subalpine Basin (SE France) and its bearing on a probable tectonic pulse on a larger scale. Cretaceous Research 72, 39–65. https://doi.org/10.1016/j.cretres.2016.11.009.
Gross, O., 2000. Influence of temperature, oxygen and food availability on the migrational activity of bathyal benthic foraminifera: evidence by microcosm experiments. In: Liebezeit, G., Dittmann, S., Kröncke, I. (Eds.), Life at Interfaces and Under Extreme Conditions. Springer Netherlands, Dordrecht, pp. 123–137. https://doi.org/10.1007/978-94-011-4148-2_12.

Haig, D.W., Mory, A.J., Dixon, M., Backhouse, J., Campbell, R.J., Ghori, K.A.R., Howe, R.W., Morris, P.A., 2004. GSWA Boologooro 1 Well Compeltion Report (Interpretive), Southern Carnarvon Basin, Wester Australia. Record 2004/4.
Hammer, O., Harper, D.A.T., Ryan, P.D., 2001. PAST: Paleontological Statistics Software Package for Education and Data Analysis, vol. 9.
Hanebuth, T.J.J., Lantzsch, H., 2008. A Late Quaternary sedimentary shelf system under hyperarid conditions: unravelling climatic, oceanographic and sea-level controls (Golfe d'Arguin, Mauritania, NW Africa). Marine Geology 256, 77–89. https://doi.org/10.1016/j.margeo.2008.10.001.
Haq, B.U., 2014. Cretaceous eustasy revisited. Global and Planetary Change 113, 44–58. https://doi.org/10.1016/j.gloplacha.2013.12.007.
Haq, B.U., Hardenbol, J., Vail, P.R., 1987. Chronology of fluctuating sea levels since the Triassic. Science 235 (4793), 1156–1167.
Harry, D.L., Tejada, M.L.G., Lee, E.Y., Wolfgring, E., Wainman, C.C., Brumsack, H.-J., Schnetger, B., Kimura, J.-I., Riquier, L., Borissova, I., Hobbs, R.W., Jiang, T., Li, Y., Maritati, A., Martinez, M., Richter, C., Tagliaro, G., White, L.T., 2020. Evolution of the Southwest Australian rifted continental margin during breakup of East Gondwana: results from International Ocean Discovery Program Expedition 369. Geochemistry, Geophysics, Geosystems 21. https://doi.org/10.1029/2020GC009144.
Hasegawa, T., Crampton, J.S., Schiøler, P., Field, B., Fukushi, K., Kakizaki, Y., 2013. Carbon isotope stratigraphy and depositional oxia through Cenomanian/Turonian boundary sequences (Upper Cretaceous) in New Zealand. Cretaceous Research 40, 61–80. https://doi.org/10.1016/j.cretres.2012.05.008.
Haug, G.H., Hughen, K.A., Sigman, D.M., Peterson, L.C., Röhl, U., 2001. Southward migration of the intertropical convergence zone through the Holocene. Science 293, 1304–1308. https://doi.org/10.1126/science.1059725.
Heimhofer, U., Wucherpfennig, N., Adatte, T., Schouten, S., Schneebeli-Hermann, E., Gardin, S., Keller, G., Kentsch, S., Kujau, A., 2018. Vegetation response to exceptional global warmth during Oceanic Anoxic Event 2. Nature Communications 9, 3832. https://doi.org/10.1038/s41467-018-06319-6.
Herrle, J.O., Pross, J., Friedrich, O., Kößler, P., Hemleben, C., 2003. Forcing mechanisms for middle-Cretaceous black shale formation: evidence from the Upper Aptian and Lower Albian of the Cocontian Basin (SE France). Palaeogeography, Palaeoclimatology, Palaeoecology 190, 399–426.
Hill, M.O., Gauch, H.G., 1980. Detrended correspondence analysis: an improved ordination technique. Vegetatio 42, 47–58.
Holbourn, A., 2001. Benthic foraminifers from lower albian black shales (site 1049, ODP LEG 171): evidence for a non "uniformitarian" record. Journal of Foraminiferal Research 31, 60–74. https://doi.org/10.2113/0310060.
Holbourn, A., Kuhnt, W., 2002. Cenomanian–Turonian palaeoceanographic change on the Kerguelen Plateau: a comparison with Northern Hemisphere records. Cretaceous Research 23, 333–349. https://doi.org/10.1006/cres.2002.1008.
Holbourn, A., Moullade, M., 1998. Lower Cretaceous Benthic Foraminifer Assemblages, Equatorial Atlantic: Biostratigraphic, Paleoenvironmental, and Paleobiogeographic Significance, vol. 159, pp. 347–362. https://doi.org/10.2973/odp.proc.sr.159.033.1998.
Howe, R.W., Haig, D.W., Apthorpe, M.C., 2000. Cenomanian-Coniacian transition from siliciclastic to carbonate marine deposition, Giralia Anticline, Southern Carnarvon Platform, Western Australia. Cretaceous Research 21, 517–551.
Huber, B.T., Hobbs, R.W., Bogus, K.A., 2019a. Expedition 369 Scientists. In: Australia Cretaceous Climate and Tectonics, Proceedings of the International Ocean Discovery Program. International Ocean Discovery Program, vol. 369. https://doi.org/10.14379/iodp.proc.369.2019.
Huber, B.T., Hobbs, R.W., Bogus, K.A., Batenburg, S.J., Brumsack, H.-J., do Monte Guerra, R., Edgar, K.M., Edvardsen, T., Garcia Tejada, M.L., Harry, D.L., Hasegawa, T., Haynes, S.J., Jiang, T., Jones, M.M., Kuroda, J., Lee, E.Y., Li, Y.-X., MacLeod, K.G., Maritati, A., Martinez, M., O'Connor, L.K., Petrizzo, M.R., Quan, T.M., Richter, C., Riquier, L., Tagliaro, G.T., Wainman, C.C., Watkins, D.K., White, L.T., Wolfgring, E., Xu, Z., 2019b. Expedition 369 methods, 2019. expedition 369 methods. In: Proceedings of the International Ocean Discovery Program. International Ocean Discovery Program, pp. 1–40.
Hull, P.M., Norris, R.D., 2011. Diverse patterns of ocean export productivity change across the Cretaceous-Paleogene boundary: new insights from biogenic barium. Paleoceanography 26, PA3205. https://doi.org/10.1029/2010PA002082.
Jarvis, I., Lignum, J.S., Gröcke, D.R., Jenkyns, H.C., Pearce, M.A., 2011. Black shale deposition, atmospheric CO_2 drawdown, and cooling during the Cenomanian-Turonian Oceanic Anoxic Event: CO_2 drawdown and cooling during OAE2. Paleoceanography 26, n. https://doi.org/10.1029/2010PA002081.
Jenkyns, H.C., 2003. Evidence for rapid climate change in the Mesozoic–Palaeogene greenhouse world. Philosophical Transactions: Mathematical, Physical and Engineering Sciences 361, 1885–1916. https://doi.org/10.1098/rsta.2003.1240.
Jenkyns, H.C., 2010. Geochemistry of oceanic anoxic events: review. Geochemistry, Geophysics, Geosystems 11. https://doi.org/10.1029/2009GC002788.
Jenkyns, H.C., Dickson, A.J., Ruhl, M., Boorn, S.H.J.M., 2017. Basalt-seawater interaction, the Plenus Cold Event, enhanced weathering and geochemical change: deconstructing Oceanic Anoxic Event 2 (Cenomanian–Turonian, Late Cretaceous). Sedimentology 64, 16–43. https://doi.org/10.1111/sed.12305.
Jones, R.W., Charnock, M.A., 1985. "Morphogroups" of agglutinating foraminifera. Their life positions and feeding habits and potential applicability in (paleo) ecological studies. Revue de Paleobiologie 4, 311–320.
Jorissen, F.J., Fontanier, C., Thomas, E., 2007. chapter seven paleoceanographical proxies based on deep-sea benthic foraminiferal assemblage characteristics. In: Developments in Marine Geology. Elsevier, pp. 263–325. https://doi.org/10.1016/S1572-5480(07)01012-3.
Kaiho, K., 1994. Benthic foraminiferal dissolved-oxygen index and dissolved-oxygen levels in the modern ocean. Geology 22, 719. https://doi.org/10.1130/0091-7613(1994)022<0719:BFDOIA>2.3.CO.
Kaiho, K., Takeda, K., Petrizzo, M.R., Zachos, J.C., 2006. Anomalous shifts in tropical Pacific planktonic and benthic foraminiferal test size during the Paleocene–Eocene thermal maximum. Palaeogeography, Palaeoclimatology, Palaeoecology 237, 456–464. https://doi.org/10.1016/j.palaeo.2005.12.017.
Kalanat, B., Vahidinia, M., Vaziri-Moghaddam, H., Mahmudy-Gharaie, M.H., Kumon, F., 2017. Benthic foraminiferal response to environmental changes across Cenomanian/Turonian boundary (OAE2) in the northeastern Tethys, Kopet-Dagh basin. Journal of African Earth Sciences 134, 33–47. https://doi.org/10.1016/j.jafrearsci.2017.05.019.
Kaminski, M.A., Boersma, E., Tyszka, J., Holbourn, A.E.L., 1995. Response of deep-water agglutinated foraminifera to dysoxic conditions in the California Borderland basins. In: Proc. Fourth Int. Workshop Agglutinated Foraminifera Sept. 12-19 1993, Grzybowski Foundation Special Publication, vol. 3, pp. 131–140.
Kaminski, M.A., Kuhnt, W., Moullade, M., 1999. The evolution and paleobiogeography of abyssal agglutinated foraminifera since the Early Cretaceous: a tale of four faunas. Neues Jahrbuch für Geologie und Palaontologie – Abhandlungen 212, 401–439. https://doi.org/10.1127/njgpa/212/1999/401.
Kauffman, E.G., Harries, P.J., 1966. The importance of crisis progenitors in recovery from mass extinction. In: Hart, M.B. (Ed.), Biotic Recovery from Mass Extinction Events, Geol. Soc. Special Publication, vol. 102, pp. 15–39.
Keller, G., Nagori, M.L., Chaudhary, M., Reddy, A.N., Jaiprakash, B.C., Spangenberg, J.E., Mateo, P., Adatte, T., 2021. Cenomanian-Turonian sea-level transgression and OAE2 deposition in the Western Narmada Basin, India. Gondwana Research 94, 73–86. https://doi.org/10.1016/j.gr.2021.02.013.
Klump, J., Hebbeln, D., Wefer, G., 2000. The impact of sediment provenance on barium-based productivity estimates. Marine Geology 169 (3–4), 259–271.
Korchagin, O.A., 2004. On events of the Terminal Cenomanian in the eastern Central Asia. Russian Journal of Earth Sciences 6, 355–377. https://doi.org/10.2205/2004ES000156.
Koutsoukos, E.A.M., 1989 (Ph.D. thesis). Middle- to Late Cretaceous Microbiostratigraphy, Palaeo-ecology and Paleogeography of the Sergipe Basin, Northeastern Brazil, vols. 1 & 2. University of Plymouth, United Kingdom, p. 886. Open Access repository at: http://hdl.handle.net/10026.1/2016.
Koutsoukos, E.A.M., Hart, M.B., 1990. Cretaceous foraminiferal morphogroup distribution patterns, palaeocommunities and trophic structures: a case study from the Sergipe Basin, Brazil. Transactions of the Royal Society of Edinburgh: Earth Sciences 81, 221–246.
Koutsoukos, E.A.M., Leary, P.N., Hart, M.B., 1990. Latest Cenomanian—earliest Turonian low-oxygen tolerant benthonic foraminifera: a case-study from the Sergipe basin (N.E. Brazil) and the western Anglo-Paris basin (southern England). Palaeogeography, Palaeoclimatology, Palaeoecology 77, 145–177. https://doi.org/10.1016/0031-0182(90)90130-Y.
Kuhnt, W., Moullade, M., Kaminski, M.A., 1996. Ecological structuring and evolution of deep sea agglutinated foraminifera — a review. Revue de Micropaléontologie 39, 271–281. https://doi.org/10.1016/S0035-1598(96)90119-1.
Kuhnt, W., Holbourn, A.E., Beil, S., Aquit, M., Krawczyk, T., Flögel, S., Chellai, E.H., Jabour, H., 2017. Unraveling the onset of Cretaceous Oceanic Anoxic Event 2 in an extended sediment archive from the Tarfaya-Laayoune Basin, Morocco: Tarfaya OAE2 Onset. Paleoceanography 32, 923–946. https://doi.org/10.1002/2017PA003146.
Kuroda, J., Ogawa, N., Tanimizu, M., Coffin, M., Tokuyama, H., Kitazato, H., Ohkouchi, N., 2007. Contemporaneous massive subaerial volcanism and late cretaceous Oceanic Anoxic Event 2. Earth and Planetary Science Letters 256, 211–223. https://doi.org/10.1016/j.epsl.2007.01.027.
Kuypers, M.M.M., Pancost, R.D., Nijenhuis, I.A., Sinninghe Damsté, J.S., 2002. Enhanced productivity led to increased organic carbon burial in the euxinic North Atlantic basin during the late Cenomanian oceanic anoxic event: enhanced productivity during C/T OAE-2. Paleoceanography 17 (3–1), 3–13. https://doi.org/10.1029/2000PA000569.
Larson, R.L., 1991. Latest pulse of earth: evidence for a middle-Cretaceous superplume. Geology 19, 547. https://doi.org/10.1130/0091-7613(1991)019<0547:LPOEEF>2.3.CO;2.
Leckie, R.M., Olson, H.C., 2003. Foraminifera as Proxies for Sea-level Change on Siliciclastic Margins, vol. 75. SEPM (Society for Sedimentary Geology) Special Publication, pp. 5–19.
Leckie, R.M., Yuretich, R.F., West, O.L., Finkelstein, D., Schmidt, M., 1998. Paleoceanography of the southwestern Western Interior Sea during the time of the Cenomanian-Turonian boundary (Late Cretaceous).
Leckie, R.M., Bralower, T.J., Cashman, R., 2002. Oceanic anoxic events and plankton evolution: biotic response to tectonic forcing during the middle-Cretaceous: oceanic anoxic events and plankton evolution. Paleoceanography 17 (13–1), 13–29. https://doi.org/10.1029/2001PA000623.
Lee, E.Y., Wolfgring, E., Tejada, M.L.G., Harry, D.L., Wainman, C.C., Chun, S.S., Schnetger, B., Brumsack, H.-J., Maritati, A., Martinez, M., Richter, C., Li, Y.-X., Riquier, L., MacLeod, K.G., Waller, T.R., Borissova, I., Petrizzo, M.R., Huber, B.T., Kim, Y., 2020. Early Cretaceous subsidence of the Naturaliste Plateau defined by a new record of volcaniclastic-rich sequence at IODP site U1513. Gondwana Research 82, 1–11. https://doi.org/10.1016/j.gr.2019.12.007.

Lowery, C.M., Bralower, T.J., 2022. Elevated post K-Pg export productivity in the Gulf of Mexico and Caribbean. Paleoceanography and Paleoclimatology 37, e2021PA004400. https://doi.org/10.1029/2021PA004400.
Lowery, C.M., Leckie, R.M., 2017. Biostratigraphy of the Cenomanian–turonian Eagle Ford Shale of South Texas. Journal of Foraminiferal Research 47, 105–128. https://doi.org/10.2113/gsjfr.47.2.105.
Lowery, C.M., Corbett, M.J., Leckie, R.M., Watkins, D., Miceli Romero, A., Pramudito, A., 2014. Foraminiferal and nannofossil paleoecology and paleoceanography of the Cenomanian–Turonian Eagle Ford Shale of southern Texas. Palaeogeography, Palaeoclimatology, Palaeoecology 413, 49–65. https://doi.org/10.1016/j.palaeo.2014.07.025.
Miller, K.G., Kominz, M.A., Browning, J.V., Wright, J.D., Mountain, G.S., Katz, M.E., Sugarman, P.J., Cramer, B.S., Christie-Blick, N., Pekar, S.F., 2005. The Phanerozoic record of global sea-level change. Science 310, 1293–1298. https://doi.org/10.1126/science.1116412.
Mort, H., Jacquat, O., Adatte, T., Steinmann, P., Föllmi, K., Matera, V., Berner, Z., Stüben, D., 2007. The Cenomanian/Turonian anoxic event at the Bonarelli level in Italy and Spain: enhanced productivity and/or better preservation? Cretaceous Research 28, 597–612. https://doi.org/10.1016/j.cretres.2006.09.003.
Murray, J.W., 2006. Ecology and Applications of Benthic Foraminifera. Cambridge University Press, Cambridge. https://doi.org/10.1017/CBO9780511535529.
Murray, J., Alve, E., 2000. Major aspects of foraminiferal variability (standing crop and biomass) on a monthly scale in an intertidal zone. Journal of Foraminiferal Research 30, 177–191. https://doi.org/10.2113/0300177.
Murray, J.W., Alve, E., 2011. The distribution of agglutinated foraminifera in NW European seas: baseline data for the interpretation of fossil assemblages. Palaeontologia Electronica 14, 41.
Murray, J.W., Alve, E., Jones, R.W., 2011. A new look at modern agglutinated benthic foraminiferal morphogroups: their value in palaeoecological interpretation. Palaeogeography, Palaeoclimatology, Palaeoecology 309, 229–241.
Neuhuber, S., Gier, S., Hohenegger, J., Wolfgring, E., Spötl, C., Strauss, P., Wagreich, M., 2016. Palaeoenvironmental changes in the northwestern Tethys during the Late Campanian Radotruncana calcarata Zone: Implications from stable isotopes and geochemistry. Chemical Geology 420, 280–296. https://doi.org/10.1016/j.chemgeo.2015.11.023.
Nguyen, T.M.P., Petrizzo, M.R., Speijer, R.P., 2009. Experimental dissolution of a fossil foraminiferal assemblage (Paleocene–Eocene Thermal Maximum, Dababiya, Egypt): implications for paleoenvironmental reconstructions. Marine Micropaleontology 73, 241–258. https://doi.org/10.1016/j.marmicro.2009.10.005.
Niebuhr, B., Baldschuhn, R., Ernst, G., Walaszczyk, I., Weiss, W., Wood, C.J., 1999. The Upper Cretaceous succession (CenomanianSantonian) of the Staffhorst Shaft, Lower Saxony, northern Germany: integrated biostratigraphic, lithostratigraphic and downhole geophysical log data. Acta Geologica Polonica 49, 175–213.
Nyong, E.E., Olsson, R.K., 1984. A paleoslope model of Campanian-lower Maestrichtian foraminifera in the North American Basin and adjacent continental margin. Marine Micropaleontology 8 (188/84), 437–477.
Ohkouchi, N., Kuroda, J., Taira, A., 2015. The origin of Cretaceous black shales: a change in the surface ocean ecosystem and its triggers. Proceedings of the Japan Academy, Series B 91, 273–291. https://doi.org/10.2183/pjab.91.273.
Owens, J.D., Gill, B.C., Jenkyns, H.C., Bates, S.M., Severmann, S., Kuypers, M.M.M., Woodfine, R.G., Lyons, T.W., 2013. Sulfur isotopes track the global extent and dynamics of euxinia during Cretaceous Oceanic Anoxic Event 2. Proceedings of the National Academy of Sciences of the United States of America 110, 18407–18412. https://doi.org/10.1073/pnas.1305304110.
Oxanen, J., Minchin, P.R., 1997. Instability of ordination results under changes in input data order: explanations and remedies. Journal of Vegetation Science 8, 447–454.
O'Connor, L.K., Jenkyns, H.C., Robinson, S.A., Remmelzwaal, S.R.C., Batenburg, S.J., Parkinson, I.J., Gale, A.S., 2020. A re-evaluation of the Plenus Cold Event, and the links between CO_2, temperature, and seawater chemistry during OAE 2. Paleoceanography and Paleoclimatology 35. https://doi.org/10.1029/2019PA003631.
Pancost, R.D., Crawford, N., Magness, S., Turner, A., Jenkyns, H.C., Maxwell, J.R., 2004. Further evidence for the development of photic-zone euxinic conditions during Mesozoic oceanic anoxic events. Journal of the Geological Society 161, 353–364. https://doi.org/10.1144/0016764903-059.
Parente, M., Frijia, G., Di Lucia, M., Jenkyns, H.C., Woodfine, R.G., Baroncini, F., 2008. Stepwise extinction of larger foraminifers at the Cenomanian-Turonian boundary: a shallow-water perspective on nutrient fluctuations during Oceanic Anoxic Event 2 (Bonarelli Event). Geology 36, 715. https://doi.org/10.1130/G24893A.1.
Paul, C.R.C., Lamolda, M.A., Mitchell, S.F., Vaziri, M.R., Gorostidi, A., Marshall, J.D., 1999. The Cenomanian–Turonian boundary at Eastbourne (Sussex, UK): a proposed European reference section. Palaeogeography, Palaeoclimatology, Palaeoecology 150, 83–121. https://doi.org/10.1016/S0031-0182(99)00009-7.
Peryt, D., Alegret, L., Molina, E., 2004. Agglinated foraminifera and their response to the Cretaceous/Paleogene (K/P) boundary event at Ain Settara, Tunisia. In: Bubik, M., Kaminski, M.A. (Eds.), Proceedings of the Sixth International Workshop on Agglutinated Foraminifera, vol. 8. Grzybowski Foundation Special Publication, pp. 393–412.
Petrizzo, M.R., Watkins, D.K., MacLeod, K.G., Hasegawa, T., Huber, B.T., Batenburg, S.J., Kato, T., 2021a. Exploring the paleoceanographic changes registered by planktonic foraminifera across the Cenomanian-Turonian boundary interval and Oceanic Anoxic Event 2 at southern high latitudes in the Mentelle Basin (SE Indian Ocean). Global and Planetary Change 206, 103595. https://doi.org/10.1016/j.gloplacha.2021.103595.
Petrizzo, M.R., Watkins, D.K., MacLeod, K.G., Hasegawa, T., Huber, B.T., Batenburg, S.J., Kato, T., 2021b. Paleoceanographic reconstructions from planktonic foraminifera across the Cenomanian/Turonian boundary and OAE 2 at southern high latitudes (IODP Site U1516, Mentelle Basin, Indian Ocean, SW Australia). In: EGU General Assembly 2021, online, 19–30 Apr 2021, EGU21-10923. https://doi.org/10.5194/egusphere-egu21-10923.
Petrizzo, M.R., Amaglio, G., Watkins, D.K., MacLeod, K.G., Huber, B.T., Hasegawa, T., Wolfgring, E., 2022. Biotic and paleoceanographic changes across the Late Cretaceous Oceanic Anoxic Event 2 in the Southern High Latitudes (IODP Sites U1513 and U1516, SE Indian Ocean). Paleoceanography and Paleoclimatology 37. https://doi.org/10.1029/2022PA004474.
Poulsen, C.J., Barron, E.J., Peterson, W.H., Wilson, P.A., 1999. A reinterpretation of Middle-Cretaceous shallow marine temperatures through model-data comparison. Paleoceanography 14, 679–697. https://doi.org/10.1029/1999PA900034.
Quilty, P.G., 1992. Upper cretaceous benthic foraminifers and paleoenvironments, southern Kerguelen Plateau, Indian Ocean. In: Wise Jr., S.W., Schlich, R., et al. (Eds.), Proceedings of the Ocean Drilling Program, Scientific Results, vol. 120, pp. 393–443.
R Core Team, 2022. R: A language and environment for statistical computing. R Found. Stat. Comput., Vienna Austria Vienna.
Reolid, M., Sebane, A., Rodríguez-Tovar, F.J., Marok, A., 2012. Foraminiferal morphogroups as a tool to approach the Toarcian Anoxic Event in the Western Saharan Atlas (Algeria). Palaeogeography, Palaeoclimatology, Palaeoecology 323–325, 87–99. https://doi.org/10.1016/j.palaeo.2012.01.034.
Reolid, M., Sánchez-Quiñónez, C.A., Alegret, L., Molina, E., 2016. The biotic crisis across the Oceanic Anoxic Event 2: palaeoenvironmental inferences based on foraminifera and geochemical proxies from the South Iberian Palaeomargin. Cretaceous Research 60, 1–27. https://doi.org/10.1016/j.cretres.2015.10.011.
Robinson, S.A., Heimhofer, U., Hesselbo, S.P., Petrizzo, M.R., 2017. Mesozoic climates and oceans – a tribute to Hugh Jenkyns and Helmut Weissert. Sedimentology 64, 1–15. https://doi.org/10.1111/sed.12349.
Rullkötter, J., Littke, R., Radke, M., Disko, U., Horsfield, B., Thurow, J., 1992. Petrography and geochemistry of organic matter in Triassic and Cretaceous deep-sea sediments from the Wombat and Exmouth plateaus and nearby abyssal plalins off Northwest Australia. In: Von Rad U Haq BU Al Proc. Ocean Drill. Program Sci. Result, Vol 122, pp. 317–333.
Sageman, B.B., Meyers, S.R., Arthur, M.A., 2006. Orbital time scale and new C-isotope record for Cenomanian-Turonian boundary stratotype. Geology 34, 125. https://doi.org/10.1130/G22074.1.
Schlanger, S.O., Jenkyns, H.C., 1976. Cretaceous oceanic anoxic events: causes and consequences. Geologie en Mijnbouw 55, 179–184.
Schlanger, S.O., Arthur, M.A., Jenkyns, H.C., Scholle, P.A., 1987. The Cenomanian-Turonian Oceanic Anoxic Event, I. Stratigraphy and distribution of organic carbon-rich beds and the marine d13C excursion. Geological Society, London, Special Publications 26 (1), 371–399, 26, 29.
Schmiedl, G., Mackensen, A., Müller, P.J., 1997. Recent benthic foraminifera from the eastern South Atlantic Ocean: dependence on food supply and water masses. Marine Micropaleontology 32, 249–287. https://doi.org/10.1016/S0377-8398(97)00023-6.
Scholle, P.A., Arthur, M.A., 1980. Carbon isotope fluctuations in Cretaceous pelagic limestones: potential stratigraphic and petroleum exploration tool. AAPG Bulletin 64, 67–87.
Setoyama, E., Kaminski, M.A., Tyszka, J., 2017. Late Cretaceous–Paleogene foraminiferal morphogroups as palaeoenvironmental tracers of the rifted Labrador margin, northern proto-Atlantic. In: Kaminski, M.A., Alegret, L. (Eds.), Proceedings of the Ninth International Workshop on Agglutinated Foraminifera, vol. 22. Grzybowski Foundation Special Publication, pp. 179–220.
Shannon, C.E., Weaver, W., 1949. The Mathematical Theory of Communication. The University of Illinois Press, Urbana, IL, pp. 1–117.
Sierro, F.J., Flores, J.A., Francés, G., Vazquez, A., Utrilla, R., Zamarreño, I., Erlenkeuser, H., Barcena, M.A., 2003. Orbitally-controlled oscillations in planktic communities and cyclic changes in western Mediterranean hydrography during the Messinian. Palaeogeography, Palaeoclimatology, Palaeoecology 190, 289–316. https://doi.org/10.1016/S0031-0182(02)00611-9.
Sikora, P.J., Olsson, R.K., 1991. A paleoslope model of late Albian to early Turonian foraminifera of the western Atlantic margin and North Atlantic basin. Marine Micropaleontology 18, 25–72.
Simpson, E.H., 1949. Measurement of diversity. Nature 163. https://doi.org/10.1038/163688a0, 688–688.
Sinninghe Damsté, J.S., van Bentum, E.C., Reichart, G.-J., Pross, J., Schouten, S., 2010. A CO_2 decrease-driven cooling and increased latitudinal temperature gradient during the middle-Cretaceous Oceanic Anoxic Event 2. Earth and Planetary Science Letters 293, 97–103. https://doi.org/10.1016/j.epsl.2010.02.027.
Sliter, W.V., 1975. Foraminiferal life and residue assemblages from Cretaceous slope deposits. GSA Bull 86, 897–906.
Takashima, R., Nishi, H., Hayashi, K., Okada, H., Kawahata, H., Yamanaka, T., Fernando, A.G., Mampuku, M., 2009. Litho-, bio- and chemostratigraphy across the Cenomanian/Turonian boundary (OAE 2) in the Vocontian Basin of southeastern France. Palaeogeography, Palaeoclimatology, Palaeoecology 273, 61–74. https://doi.org/10.1016/j.palaeo.2008.12.001.

Tewari, A., Hart, M.B., Watkinson, M.P., 1996. Foraminiferal recovery after the middle-Cretaceous oceanic anoxic events (OAEs) in the Cauvery Basin, south-east India. Geological Society, London, Special Publications 102, 237–244. https://doi.org/10.1144/GSL.SP.1996.001.01.17.

Thurow, J., Brumsack, H.-J., Rullkötter, J., Littke, R., Meyers, P., 2013. The Cenomanian/Turonian Boundary Event in the Indian Ocean: a key to understand the global picture. In: Duncan, R.A., Rea, D.K., Kidd, R.B., von Rad, U., Weissel, J.K. (Eds.), Geophysical Monograph Series. American Geophysical Union, Washington, D. C., pp. 253–273. https://doi.org/10.1029/GM070p0253

Trabucho Alexandre, J., Tuenter, E., Henstra, G.A., van der Zwan, K.J., van de Wal, R.S.W., Dijkstra, H.A., de Boer, P.L., 2010. The middle-Cretaceous North Atlantic nutrient trap: Black shales and OAEs: middle-Cretaceous n. Atlantic nutrient trap. Paleoceanography 25. https://doi.org/10.1029/2010PA001925.

Tsikos, H., Jenkyns, H.C., Walsworth-Bell, B., Petrizzo, M.R., Forster, A., Kolonic, S., Erba, E., Premoli Silva, I., Baas, M., Wagner, T., Sinninghe Damsté, J.S., 2004. Carbon-isotope stratigraphy recorded by the Cenomanian–Turonian Oceanic Anoxic Event: correlation and implications based on three key localities. Journal of the Geological Society 161, 711–719. https://doi.org/10.1144/0016-764903-077.

Turgeon, S.C., Creaser, R.A., 2008. Cretaceous oceanic anoxic event 2 triggered by a massive magmatic episode. Nature 454, 323–326. https://doi.org/10.1038/nature07076.

Tyszka, J., 1994. Response of middle Jurassic benthic foraminiferal morphogroups to dysoxic/anoxic conditions in the Pieniny Klippen Basin, Polish Carpathians. Palaeogeography, Palaeoclimatology, Palaeoecology 110, 55–81. https://doi.org/10.1016/0031-0182(94)90110-4.

van Bentum, E.C., Reichart, G.-J., Forster, A., Sinninghe Damsté, J.S., 2012. Latitudinal differences in the amplitude of the OAE-2 carbon isotopic excursion: pCO_2 and paleo productivity. Biogeosciences 9, 717–731. https://doi.org/10.5194/bg-9-717-2012.

Van Wagoner, J.C., Posamentier, H.W., Mitchum, R.M., Vail, P.R., Sarg, J.F., Loutit, T.S., Hardenbol, J., 1988. An overview of sequence stratigraphy and key definitions. In: Wilgus, C.W., et al. (Eds.), Sea Level Changes: an Integrated Approach, vol. 42. Society of Economic Paleontologists and Mineralogists special publication, pp. 39–45.

Voigt, S., Gale, A.S., Voigt, T., 2006. Sea-level change, carbon cycling and palaeoclimate during the Late Cenomanian of northwest Europe; an integrated palaeoenvironmental analysis. Cretaceous Research 27, 836–858. https://doi.org/10.1016/j.cretres.2006.04.005.

Voigt, S., Erbacher, J., Mutterlose, J., Weiss, W., Westerhold, T., Wiese, F., Wilmsen, M., Wonik, T., 2008. The Cenomanian Turonian of the Wunstorf section (North Germany): global stratigraphic reference section and new orbital time scale for Oceanic Anoxic Event 2. Newsletters on Stratigraphy 43, 65–89. https://doi.org/10.1127/0078-0421/2008/0043-0065.

Wainman, C.C., Tagliaro, G., Jones, M.M., Charles, A.J., Hall, T., White, L.T., Bogus, K.A., Wolfgring, E., O'Connor, L.K., McCabe, P.J., Holford, S.P., 2020. The sedimentological evolution and petroleum potential of a very thick Upper Cretaceous marine mudstone succession from the southern high latitudes—a case study from the Bight Basin, Australia. Marine and Petroleum Geology 118, 104441. https://doi.org/10.1016/j.marpetgeo.2020.104441.

Walaszczyk, I., Kopaevich, L.F., Olferiev, A.G., 2004. Inoceramid/foraminiferal succession of the Turonian and Coniacian (Upper Cretaceous) of the Briansk region (Central European Russia). Acta Geologica Polonica 54, 569–581.

Ward, J.H., 1963. Hierarchical grouping to optimize an objective function. Journal of the American Statistical Association 58, 236–244.

Weltje, G.J., Tjallingii, R., 2008. Calibration of XRF core scanners for quantitative geochemical logging of sediment cores: Theory and application. Earth and Planetary Science Letters 274, 423–438. https://doi.org/10.1016/j.epsl.2008.07.054.

Wendler, I., Huber, B.T., MacLeod, K.G., Wendler, J.E., 2013. Stable oxygen and carbon isotope systematics of exquisitely preserved Turonian foraminifera from Tanzania — Understanding isotopic signatures in fossils. Marine Micropaleontology 102, 1–33. https://doi.org/10.1016/j.marmicro.2013.04.003.

White, L.T., Gibson, G.M., Lister, G.S., 2013. A reassessment of paleogeographic reconstructions of eastern Gondwana: bringing geology back into the equation. Gondwana Research 24, 984–998. https://doi.org/10.1016/j.gr.2013.06.009.

Widmark, J.G.V., Speijer, R.P., 1997. Benthic foraminiferal ecomarker species of the terminal Cretaceous (late Maastrichtian) deep-sea Tethys. Marine Micropaleontology 31, 135–155. https://doi.org/10.1016/S0377-8398(97)00008-X.

Wignall, P.B., Bond, D.P.G., Kuwahara, K., Kakuwa, Y., Newton, R.J., Poulton, S.W., 2010. An 80 million year oceanic redox history from Permian to Jurassic pelagic sediments of the Mino-Tamba terrane, SW Japan, and the origin of four mass extinctions. Global and Planetary Change 71, 109–123. https://doi.org/10.1016/j.gloplacha.2010.01.022.

Wolfgring, E., Amaglio, G., Petrizzo, M.R., 2023. Cenomanian/Turonian benthic foraminiferal abundance data of IODP Site U1516, Mentelle Basin, Indian Ocean. PANGAEA. https://doi.org/10.1594/PANGAEA.957995.

Wolfgring, E., Kaminski, M.A., Waśkowska, A., Wainman, C.C., Petrizzo, M.R., Lee, E.Y., Edvardsen, T., Gong, S., 2021. Foraminiferal stratigraphy and paleoenvironments of a high latitude marginal marine basin – a Late Cretaceous record from IODP Site U1512 (Great Australian Bight). Palaeogeography, Palaeoclimatology, Palaeoecology 580, 110604. https://doi.org/10.1016/j.palaeo.2021.110604.

Wolfgring, E., Petrizzo, M.R., MacLeod, K.G., Huber, B.T., Watkins, D.K., 2022. Santonian deep sea benthic foraminifera from IODP Site U1513, Mentelle Basin (SW Australia): Reactions of benthic foraminiferal assemblages to surface water cooling at southern high latitudes. Marine Micropaleontology 175, 102152. https://doi.org/10.1016/j.marmicro.2022.102152.

Zheng, X.-Y., Jenkyns, H.C., Gale, A.S., Ward, D.J., Henderson, G.M., 2013. Changing ocean circulation and hydrothermal inputs during Ocean Anoxic Event 2 (Cenomanian–Turonian): Evidence from Nd-isotopes in the European shelf sea. Earth Planet. Sci. Lett. 375, 338–348. https://doi.org/10.1016/j.epsl.2013.05.053.

Appendix A. Supplementary data

Supplementary data to this article can be found online at https://doi.org/10.1016/j.cretres.2023.105555.